catalysts

MDPI

*Review*

# The Origin of Au/$Ce_{1-x}Zr_xO_2$ Catalyst's Active Sites in Low-Temperature CO Oxidation

**Izabela Dobrosz-Gómez [1,*], Miguel-Ángel Gómez-García [2] and Jacek Michał Rynkowski [3]**

[1] Grupo de Investigación en Procesos Reactivos Intensificados y Materiales Avanzados—PRISMA, Departamento de Física y Química, Facultad de Ciencias Exactas y Naturales, Universidad Nacional de Colombia, Sede Manizales, 170004 Manizales, Colombia

[2] Grupo de Investigación en Procesos Reactivos Intensificados y Materiales Avanzados—PRISMA, Departamento de Ingeniería Química, Facultad de Ingeniería y Arquitectura, Universidad Nacional de Colombia, Sede Manizales, 170004 Manizales, Colombia; magomez@unal.edu.co

[3] Institute of General and Ecological Chemistry, Lodz University of Technology, Żeromskiego 116, 90-924 Lodz, Poland; jacek.rynkowski@p.lodz.pl

* Correspondence: idobrosz-gomez@unal.edu.co

Received: 1 October 2020; Accepted: 9 November 2020; Published: 13 November 2020


**Abstract:** Gold catalysts have found applications in many reactions of both industrial and environmental importance. Great interest has been paid to the development of new processes that reduce energy consumption and minimize pollution. Among these reactions, the catalytic oxidation of carbon monoxide (CO) is an important one, considering that a high concentration of CO in the atmosphere creates serious health and environmental problems. This paper examines the most important achievements and conclusions arising from the own authorship contributions concerning (2 wt. % Au)/$Ce_{1-x}Zr_xO_2$ catalyst's active sites in low-temperature CO oxidation. The main findings of the present review are: (1) The effect of preparing conditions on Au crystallite size, highlighting some of the fundamental underpinnings of gold catalysis: the Au surface composition and the poisoning effect of residual chloride on the catalytic activity of (2 wt. % Au)/$Ce_{1-x}Zr_xO_2$ catalysts in CO oxidation; (2) The identification of ion clusters related to gold and their effect on catalyst' surface composition; (3) The importance of physicochemical properties of oxide support (e.g., its particle size, oxygen mobility at low temperature and redox properties) in the creation of catalytic performance of Au catalysts; (4) The importance of oxygen vacancies, on the support surface, as the centers for oxygen molecule activation in CO reaction; (5) The role of moisture (200–1000 ppm) in the generation of enhanced CO conversion; (6) The Au-assisted Mars-van Krevelen (MvK) adsorption–reaction model was pertinent to describe CO oxidation mechanism. The principal role of Au in CO oxidation over (2 wt. % Au)/$Ce_{1-x}Zr_xO_2$ catalysts was related to the promotion in the transformation process of reversibly adsorbed or inactive surface oxygen into irreversibly adsorbed active species; (7) Combination of metallic gold ($Au^0$) and Au-OH species was proposed as active sites for CO adsorption. These findings can help in the optimization of Au-containing catalysts.

**Keywords:** Au/$Ce_{1-x}Zr_xO_2$ catalyst; preparation procedure; residual chlorine; Au dispersion; CO oxidation

## 1. Introduction

It is a great pleasure and honor for us to contribute to this Special Issue of the Catalysts journal dedicated to recognizing the outstanding career contributions of Professor Hugo de Lasa to the fields of heterogeneous catalysis, photocatalysis and catalytic reaction engineering. Over the years, in the subject of heterogeneous catalysis, Professor de Lasa has defined a clear path for the application of several types of catalysts, including, but not limited to, nickel-based ones, HZSM-5 zeolites, $TiO_2$ (photocatalysis)

and $Al_2O_3$ to different reactive processes. Professor de Lasa was and continues to be a constant source of inspiration for both the academic and industry sectors related to the application of chemical reaction engineering.

Gold catalysts have found applications in many reactions of both industrial and environmental importance. Great interest has been paid to the development of new processes that reduce energy consumption and minimize pollution. Among these reactions, carbon monoxide (CO) oxidation is an important one [1,2]. Moreover, CO oxidation serves as a prototypical reaction for heterogeneous catalysis. CO has no color, no smell, no taste, and it is a toxic gas at high concentrations. It is a byproduct of partial combustion of fuels in conditions of oxygen deficiency, and it is one of the main pollutants originating from internal combustion engines. It is estimated that more than 66% of the synthetic CO gas present in the air originates from automotive emissions, even if current three-way catalysts (TWCs), based on noble metals, remove 99% of CO [3]. Considering its negative impact on the environment and its high toxicity to humans and animals (due to the strong affinity to hemoglobin in the bloodstream resulting in decreasing the oxygen transport capacity of blood), CO is one of the four major air pollutants regulated both in the European Union ("Euro emissions standards") and in many other countries in the world. CO is a poison for platinum-based catalysts for proton exchange membrane fuel cells (PEMFC). Thus, before entering PEMFC, its content must be reduced to levels below 50 ppm [4]. There are several techniques suitable for CO removal, including, but not limited to, adsorption, CO methanation and catalytic oxidation. However, CO oxidation ($CO + 0.5\ O_2 \leftrightarrow CO_2$; $\Delta H^\circ = -283$ kJ/mol) is the most efficient one.

Au catalysts can be used for CO removal in $CO_2$ lasers and CO gas sensors, air-purification devices for respiratory protection, pollution control devices for reducing fixed (industrial) and mobile emission or even for removing trace quantities of CO from ambient air in enclosed atmospheres [5]. The interest in studying supported gold catalysts has increased since Haruta and coworkers discovered their extraordinary activity for low-temperature CO oxidation [6]. They reported that, compared to a highly dispersed supported Pt catalyst, the Au catalyst is much more active at temperatures below 130 °C [7]. Attention has been raised not only from the commercial implication of this discovery but also from the desire to answer the questions of why normally inert Au material can catalyze chemical reactions so efficiently.

Most studies on Au catalysts have suggested that their activity is highly sensitive to the details of the preparation procedure and catalytic testing conditions [8–12]. Metal-support interactions have a significant effect on the performance of supported gold catalysts. Additionally, their efficiency in CO oxidation at low temperatures depends on various factors, including the nature of the support, Au particle size, preparation procedure, pretreatment conditions and properties of the gold-support interface. A majority of preparation methods derive from the deposition–precipitation technique proposed by Haruta´s team [13]. High activity can originate at the gold-support interface, with the support playing a crucial role. Stable activity can result from optimizing solution aging during the preparation and low calcination temperatures. The deposition–precipitation using urea ($CO(NH_2)_2$) may be advantageous over that using NaOH [14]. Catalysts prepared using conventional impregnation result to be less active than the platinum group metal catalysts prepared in this way [15], especially when chloroauric acid is used as a precursor. The grafting methods use monodispersed Au colloids stabilized by organic ligands or polymer compounds [16]. Only the gas phase grafting technique is effective for the deposition of Au nanoparticles on activated carbon, but the size of Au particles is relatively large. Direct anionic exchange (DAE) provides a small gold particle size on $Al_2O_3$ [17] and hydrotalcite [18], both with high catalytic activity in CO oxidation.

$CeO_2$ is one of the most studied active supports due to its redox behavior achieved by easy and reversible transformation of $Ce^{4+}$ cations into $Ce^{3+}$ ones, accompanied by oxygen vacancies formation. There are several reasons for $CeO_2$ application as a catalyst component: (i) a noble metal itself, used as catalyst, is economically unsustainable (e.g., its high price); (ii) $CeO_2$ exhibits high oxygen storage (release) capacity (OSC) due to its redox properties, comparing with various metal oxides

($TiO_2$, $Fe_2O_3$, $SnO_2$, $Co_3O_4$, $MnO_x$ and $Al_2O_3$); (iii) the OSC guarantees stoichiometric composition of gases during air-to-fuel oscillation by releasing and storing oxygen under fuel-lean and fuel-rich conditions, respectively; (iv) a beneficial effect of precious metal—$CeO_2$ interactions on the activity of the redox couple $Ce^{4+}/Ce^{3+}$ with its ability to change from $Ce^{4+}$ under oxidizing conditions to $Ce^{3+}$ under net reducing conditions and vice versa; (v) $CeO_2$ is known to affect the dispersion of supported metals, promote noble metal reduction and oxidation, store and release oxygen, hydrogen and sulfur, form surface and bulk vacancies; (vi) $CeO_2$ presents oxygen vacancies giving it the ability to exchange oxygen species with the environment, converting it into a kind of an oxygen buffer with high oxygen storage capacity [19,20].

However, pure $CeO_2$ does not catalyze CO oxidation at low temperatures, and it is characterized by poor thermal stability [21,22]. It can be improved by (i) doping of $CeO_2$ fluorite lattice with metals that enhance the intrinsic activity and/or physical properties (e.g., the presence of foreign cations such as $Al^{3+}$, $Si^{4+}$ or $Zr^{4+}$ in the $CeO_2$ lattice, forming a solid solution, significantly improves the stability of the surface area and strongly enhance the redox properties of ceria) and (ii) loading of metal nanoparticles on $CeO_2$ surface that provides novel active interfacial sites between metals and $CeO_2$ surface. Thus, the expected synergetic effect between (noble) metallic nanoparticles and $CeO_2$-based materials is a promising methodology to develop active and stable catalysts for low-temperature CO oxidation [23].

Since our earlies work [21,24], we have demonstrated the effectiveness of $CeO_2$–$ZrO_2$ mixed oxides used as supports for Au nanoparticles in low-temperature CO oxidation. Their unique redox properties and high mobility of lattice oxygen, strongly depending on the Ce/Zr molar ratio, were important arguments to select $CeO_2$–$ZrO_2$ mixed oxides as support for Au nanoparticles. Furthermore, $CeO_2$ has already been known to be active for the removal of post-combustion pollutants [20]. Moreover, the last generation of commercial TWCs presented better catalytic performance when the supports contain ceria-zirconia solid solutions instead of pure $CeO_2$, as reported by Daturi et al. [25]. Finally, a similar value of the isoelectric point (IEP) for $CeO_2$, $ZrO_2$ and consequently, their mixed oxides allowed to create comparable conditions for gold deposition.

During the past decade, the latest research trends on CO oxidation are focused on several topics. The first one is related to the reduction of the high cost of noble metals and to the improvement of catalyst stability at high temperatures [26–28]. Thus, the application of single-atom catalysts (SACs), e.g., Au/$CeO_2$, able to convert CO into $CO_2$ at low temperatures, and characterized with good stability and a low price, has recently drawn considerable attention [29]. SACs unique structure can contribute to activating the adsorbed CO and $O_2$ and stabilizing the intermediates. Electron transfer between the metal atom and the support can play an important role in tuning the electronic structure, which can influence their activity, selectivity and stability [30]. The second investigation trend is related to the importance of understanding the dynamic behavior of catalytic oxidation of CO for the future development of catalytic systems [31]. Finally, the last group of topics is related to unveil the mechanism of catalytic CO oxidation. Although this reaction is considered as a relatively simple one, over 20 different mechanistic steps are proposed in the open literature [32–38]. In general, they are based on two widely accepted possible reaction pathways: Langmuir–Hinshelwood (LH) and Mars van Krevelen (MvK) [39–41]. The LH dual-site mechanism concerns competitive adsorption of CO and oxygen molecules from the gas phase on the catalyst surface, their subsequent reaction and $CO_2$ desorption to the gas phase [42]. On the other hand, in the MvK mechanism, surface lattice oxygen close to the Au nanoparticles represents the active oxygen species for CO oxidation, which reacts with CO adsorbed on the Au nanoparticles. Consequently, the reaction proceeds via the continuous formation and replenishment of surface oxygen vacancies by the reaction of the catalyst with CO and $O_2$ (Au-assisted MvK mechanism) [43].

Here, as an extension of our previous works [21–24,44–48], the detailed insight into the origin of Au/$Ce_{1-x}Zr_xO_2$ catalyst's active sites in low-temperature CO oxidation is reviewed. Special attention is paid to the factors that influence their high activity, e.g., Au crystallite size, presence of residual chloride,

catalyst surface composition, support composition, catalysts pretreatment, the relation between the physicochemical properties of the supports and the catalytic performance of Au/$Ce_{1-x}Zr_xO_2$. The catalyst's reducibility is used as a tool to determine both the support and the Au particles' chemical state and their contribution to the reaction. A conclusive analysis of the CO oxidation mechanism over Au/$Ce_{1-x}Zr_xO_2$ catalysts is also presented.

## 2. Factors Affecting CO Oxidation Reaction

### *2.1. Effect of the Preparation Conditions and the Catalyst Properties*

Details of DAE preparation procedure, see Materials and Methods section, related to the application of the washing procedure for residual chloride removal from the catalysts, significantly affect (2 wt. % Au)/$Ce_{1-x}Zr_xO_2$ catalysts properties. Residual chloride presents a poisonous effect on Au supported on $Al_2O_3$ or $TiO_2$ [49]. It can affect the catalytic activity in two different ways: (i) facilitating the agglomeration of Au particles during the calcination step by the formation of Au-Cl-Au bridges and increasing the average gold particle size; and (ii) inhibiting the catalytic activity by poisoning the active site. Its quantitative effect depends on the sample composition. The amount of adsorbed and/or incorporated chloride depends on the nature of the support, its isoelectric point and its adsorption capacity. The high affinity of $Cl^-$ for the Au active site suggests that the active site is partly cationic in nature. This section details the effect of the applied washing procedure on the properties of (2 wt. % Au)/$Ce_{1-x}Zr_xO_2$ catalysts and their performance in CO oxidation. Specifically, the real Au content, the Au particle size, the presence of residual chloride, catalyst crystallinity and morphology, and catalyst surface composition are reviewed [21,24].

Figure 1 shows that the washing procedure applied to remove residual chlorine during the catalyst preparation stage affects both the real Au content and Au particle size.

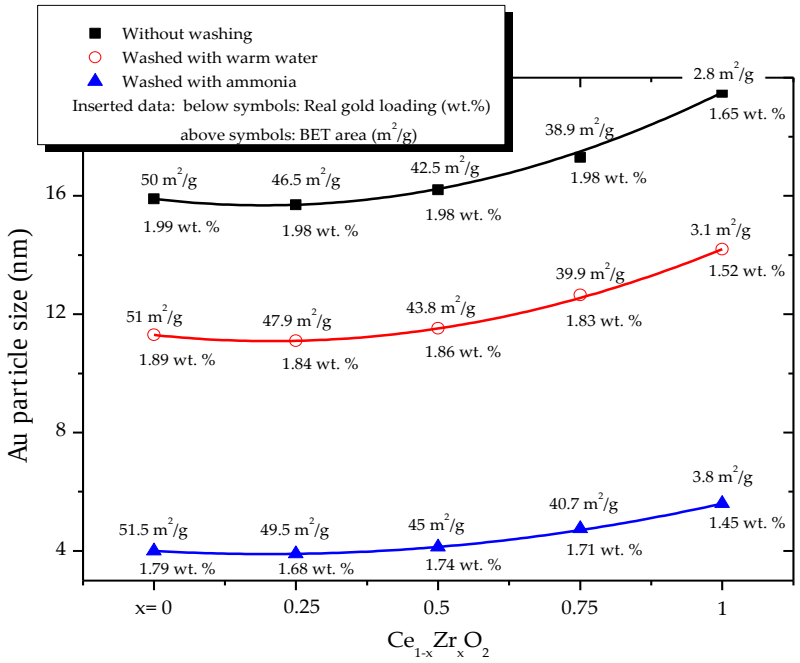


**Figure 1.** Characterization of (2 wt. % Au)/$Ce_{1-x}Zr_xO_2$ catalysts washed with different agents; below symbols: real gold-loading (wt. %); above symbols: Brunauer–Emmett–Teller (BET) -specific surface area ($m^2/g$).

All catalysts prepared without washing show the real Au content almost identical to the nominal one (2 wt. %), confirming high efficiency of the DAE preparation procedure. Only, for Au/$ZrO_2$, the real Au-loading is ca. 20% lower than the expected one. Considering strong Lewis-type acidity

of $ZrO_2$, which is beneficial to an anionic exchange, we believe that this is related to the significantly lower specific surface area of $ZrO_2$ (4.5 $m^2/g$), comparing to $CeO_2$ (58.1 $m^2/g$) and $Ce_{1-x}Zr_xO_2$ oxides (50.1 $m^2/g$, 46.5 $m^2/g$ and 41 $m^2/g$ for x equaled to 0.25, 0.5 and 0.75, respectively). Notice that subsequent washing of the catalyst with warm water or ammonia led to the loss of Au (ca. 5–10% for the catalysts washed with warm water and ca. 10–15% for catalysts washed with ammonia). This is due to: (i) the removal of non-attached gold complexes, simply adsorbed on the support surface due to the deficient quantity of hydroxyl groups available for anionic exchange; and (ii) the replacement of $Cl^-$ ligands by OH groups in the exchanged Au species [50]. We have already reported on the high efficiency of ammonia for residual chloride ions removal (e.g., their content in $Au/Mg_4Al_2$ [18] was found to be lower than 200 ppm). Independent of the washing procedure, the specific surface area of (2 wt. % Au)/$Ce_{1-x}Zr_xO_2$ catalyst is similar to that of the corresponding oxide support (Figure 1) [24].

The effect of the washing procedure on Au particle size is also resumed in Figure 1. Catalysts washed with either warm water or ammonia present Au particle size ca. 30 or 70% lower than that of catalysts prepared without washing. BSE photomicrographs, EDS maps and characteristic X-ray spectra of (2 wt. % Au)/$Ce_{0.75}Zr_{0.25}O_2$ catalysts, prepared using different washing procedures, are presented in Figure 2. Notice that the uncalcined catalyst, prepared without washing (Figure 2a), presents a more homogeneous distribution of Au than the calcined one (Figure 2b). This last one shows characteristic microareas with higher Au concentration, resulting from Au–Cl–Au bridges formation during the calcination process [51]. A similar observation was made basing on HRTEM results (Figure 3a). For $Au/CeO_2$ and $Au/Ce_{0.75}Zr_{0.25}O_2$ catalysts, prepared without washing, most Au particles ranged from 5 to 30 nm. For $Au/ZrO_2$, they were in the range of 10–35 nm. However, washing the catalysts with warm water leads to a more homogeneous distribution of Au (Figure 2c) and a decrease in the Au particle size (Figure 3b). Thus, for $Au/CeO_2$ and $Au/Ce_{0.75}Zr_{0.25}O_2$ catalysts, Au particles were in the range of 5–15 nm. For $Au/ZrO_2$, they ranged from 5 to 20 nm. Still, Au agglomerates larger than 20 nm were observed. This due to the incomplete removal of residual chlorine from the catalysts, using warm water as a washing agent. On the other hand, for the catalyst washed with ammonia (Figure 2d), neither Au agglomerations nor Au clusters were found. Moreover, the signal characteristic of $Cl^-$, observed in the X-ray spectra of catalysts prepared without washing (Figure 2a,b), is absent in the spectra of washed catalysts (Figure 2c,d). For ammonia washed $Au/CeO_2$, and $Au/Ce_{0.75}Zr_{0.25}O_2$, mostly spherical Au particles were observed in the range of 1–5 nm. For $Au/ZrO_2$, Au particle size ranged from 1 to 7 nm (Figure 3c). Thus, Au particle agglomeration, due to the presence of residual chlorine originated from $HAuCl_4.3H_2O$, can be successfully avoided using ammonia as a washing agent.

The ammonia washing procedure was more efficient for residual chlorine removal for (2 wt. % Au)/$ZrO_2$ than for both (2 wt. % Au)/$CeO_2$ and (2 wt. % Au)/$Ce_{0.75}Zr_{0.25}O_2$ (Figure 4). Moreover, for $CeO_2$-containing catalysts, both prepared without washing and washed with ammonia, the presence of $Cl^-$—containing species was more evident. This is due to a different mechanism of chloride ions incorporation into these catalysts. The $Cl^-$ can be present both in the exchanged Au species and in the support lattice. According to Force et al. [49], chloride ions can be incorporated into an oxygen vacancy of ceria (Lewis-type sites) and/or it can be exchanged with ceria's $OH^-$ groups (Brønsted-type sites). For this reason, for catalyst supported on $ZrO_2$, lower content of $Cl^-$—containing species were observed.

We used the ToF-SIMS technique to determine the effect of the washing procedure on the catalyst's surface composition [24]. Figure 4 summarizes the values of ToF-SIMS selected secondary ions intensity ratios for some (2 wt. % Au)/$Ce_{1-x}Zr_xO_2$ catalysts prepared both without washing and washed with ammonia. Ion clusters related to gold were found. For all catalysts, the presence of $Cl^-$ ions in the surrounding of Au centers (e.g., $AuCl^-$, $AuCl_2^-$, etc.) was confirmed. Catalysts prepared without washing presented the intensity ratio of $Cl^-$ ions to the total number of ions ($Cl^-$/total$^-$) significantly higher than that for the catalysts washed with ammonia. Since the average Au particle size of catalysts prepared without washing was also significantly higher than that of systems washed with ammonia (Figure 3), the role of residual chlorine in the sintering of Au can be accepted.

Moreover, for Ce-containing catalysts prepared without washing, the intensity ratio of ($Cl^-$/total$^-$), ($AuCl^-$/$Au^-$), ($AuCl_2^-$/$Au^-$) and ($AuClO^-$/$Au^-$) was significantly higher than that for (2 wt. % Au)/$ZrO_2$. This observation confirms a higher affinity of ceria to chlorine.

(**a**)

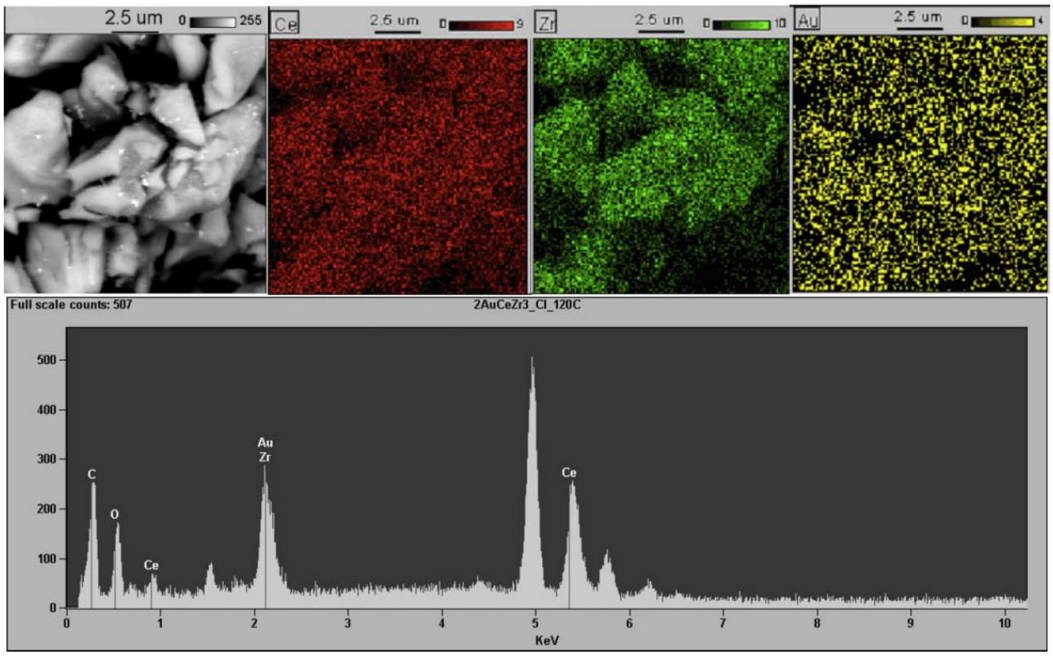


(**b**)

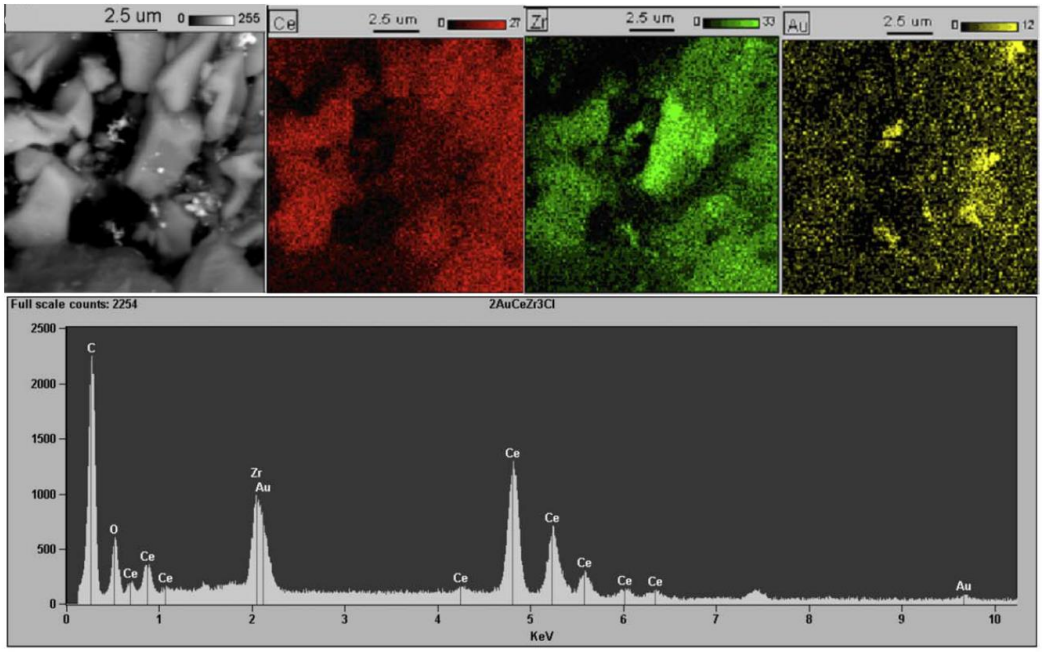


**Figure 2.** *Cont.*

(**c**)

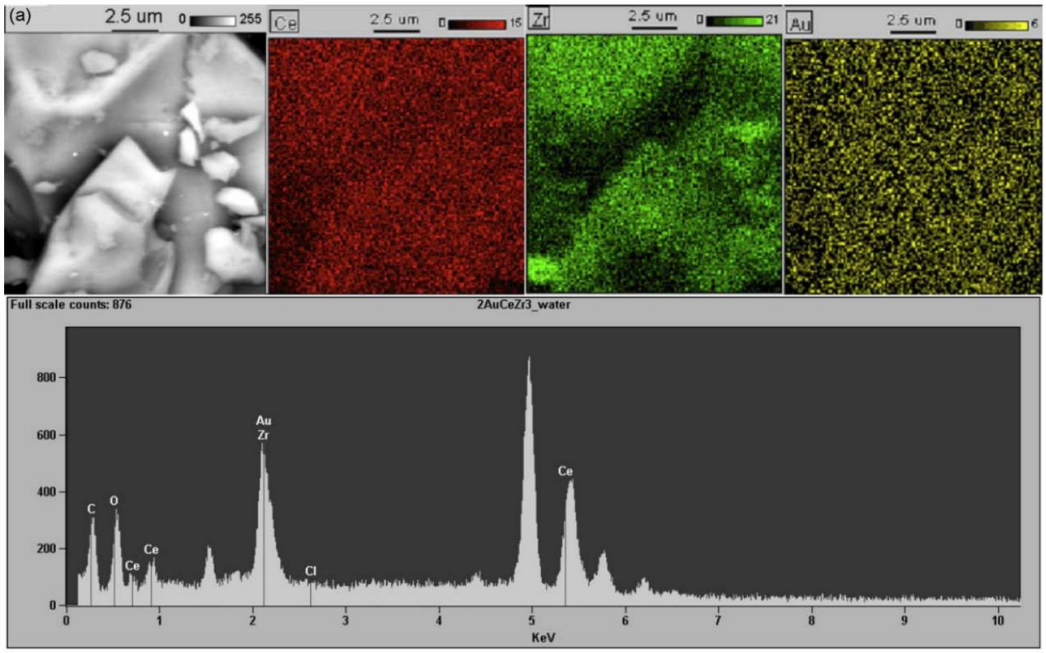


(**d**)

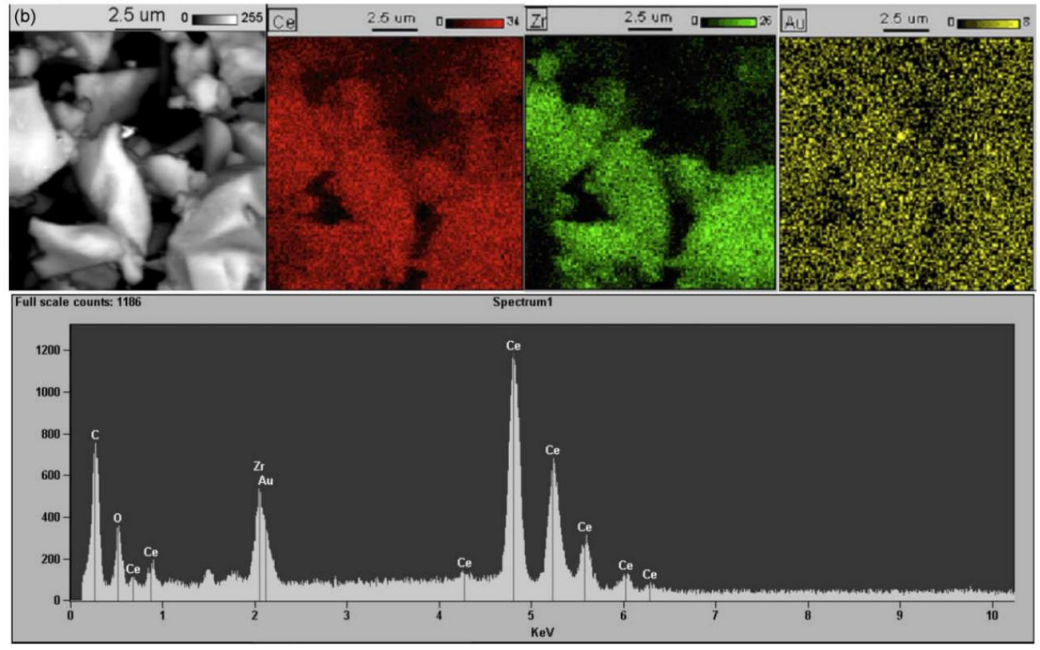


**Figure 2.** The back-scattered electron (BSE) photomicrographs, EDS maps and characteristic X-ray spectra of (2 wt. % Au)/$C_{0.75}Zr_{0.25}O_2$ catalysts washed with different agents: (**a**) without washing (dried at 120 °C), (**b**) without washing (calcined at 300 °C), (**c**) washed with warm water (calcined at 300 °C), (**d**) washed with ammonia (calcined at 300 °C). (copyright permission number 4932711312351) [24].

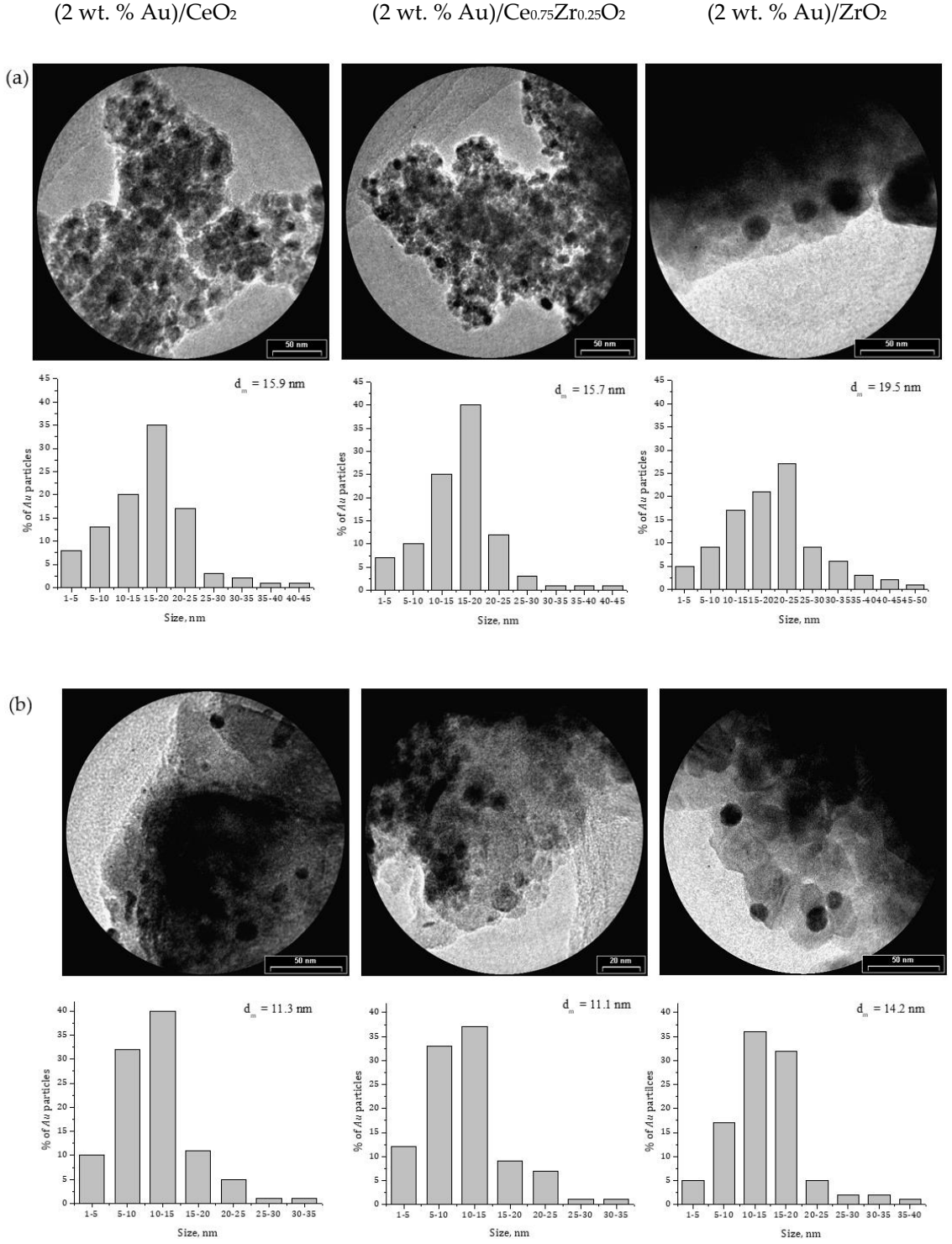


**Figure 3.** *Cont*.

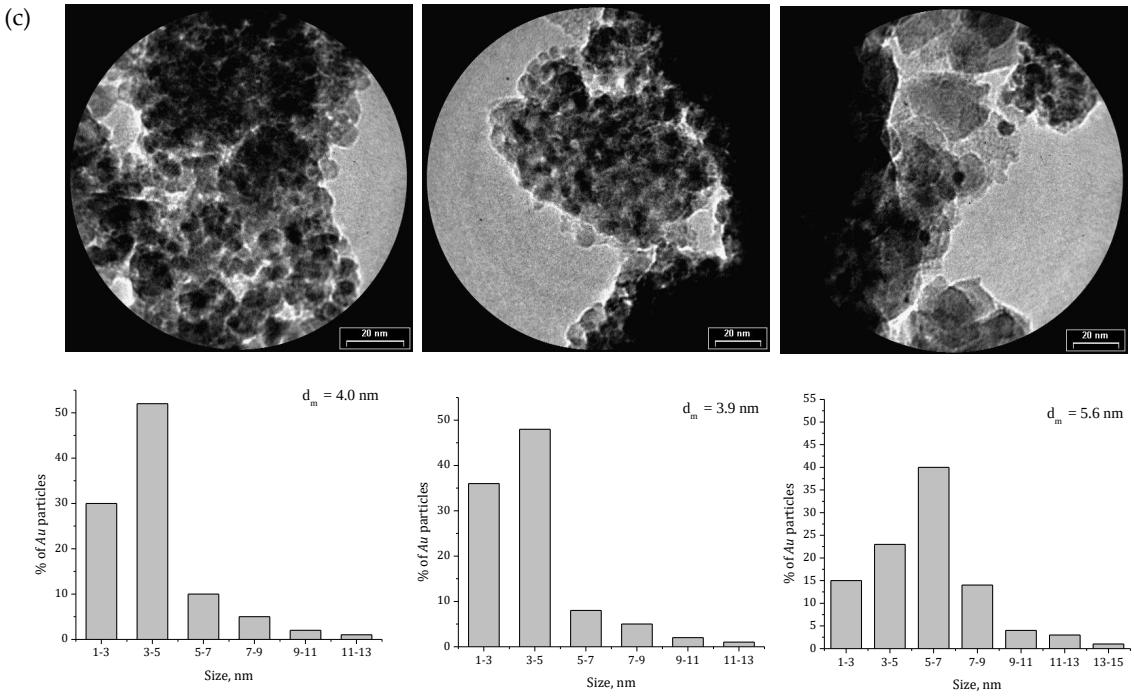


**Figure 3.** The representative HRTEM images and the histograms of Au particle size distribution of Au supported on $CeO_2$, $Ce_{0.75}Zr_{0.25}O_2$ and $ZrO_2$ washed with different agents: (**a**) prepared without washing, (**b**) washed with warm water, (**c**) washed with ammonia (**a** and **c**—copyright permission number 4932711312351) [24].

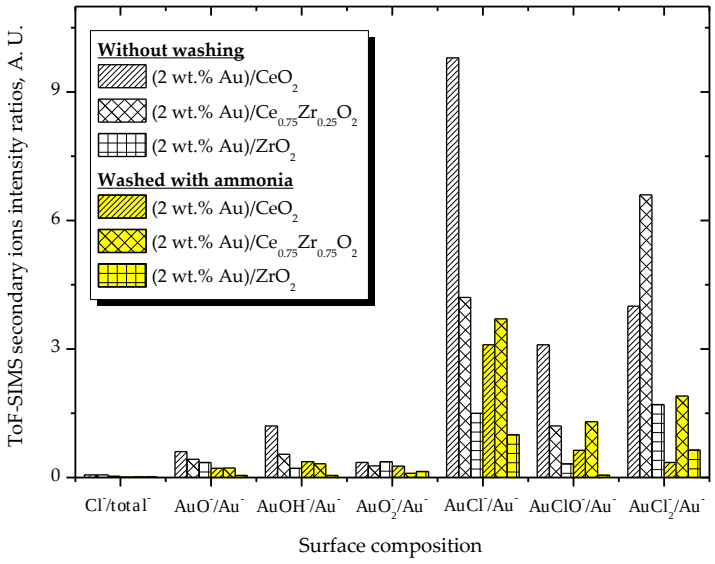


**Figure 4.** The resume of values of time-of-flight secondary ion mass spectrometry (ToF-SIMS)-selected secondary ions intensity ratios for some (2 wt. % Au)/$Ce_{1-x}Zr_xO_2$ catalysts prepared without washing and washed with ammonia.

For all studied catalysts, the presence of oxygen ions in the surrounding of gold centers ($AuO^-$, $AuO_2^-$, $AuOH^-$, etc.) was also confirmed [21,24,52]. Moreover, the intensity ratio of ($AuO^-/Au^-$), ($AuOH^-/Au^-$) and ($AuO_2^-/Au^-$) was higher for Au supported on Ce-containing oxides. Fu et al. [53], using the XPS method, confirmed the presence of different Au-containing ion clusters on Au/γ-$Al_2O_3$, Au/$TiO_2$ and on a gold foil. However, they detected only metallic Au and $AuCl^-$ ion fragments. Any ion fragments related to $AuO^-$, $AuOH^-$ and $AuO_2^-$ were found. Thus, the presence of $AuO^-$,

$AuO_2^-$ and $AuOH^-$ ion clusters points to the existence of different oxidized species of gold on (2 wt. % Au)/$Ce_{1-x}Zr_xO_2$ surface. This suggests either partial oxidation of Au or chemisorption of oxygen on gold nanoparticles. Moreover, the presence of $AuOH^-$ ion clusters indicates the chemisorption of water on Au particles [53].

The morphology of (2 wt. % Au)/$Ce_{1-x}Zr_xO_2$ catalysts was highly uniform. It strongly depended on $Ce_{1-x}Zr_xO_2$ composition [21], as confirmed by SEM–EDS technique (Figure 5). The interaction of Au precursor ($HAuCl_4.3H_2O$) with $CeO_2$ during the catalyst preparation does not lead to the aggregation of spherical grains of the oxide support (Figure 5a). Neither agglomeration of regular and plated shaped particles of $Ce_{0.75}Zr_{0.25}O_2$ (Figure 5b) nor angular particles of $ZrO_2$ was observed (Figure 5c). For all catalysts, Au was homogenously distributed on the supports surface. In general, the distribution of all elements was very uniform. Neither Au clusters nor the highly concentrated Au microareas were observed.

(**a**)

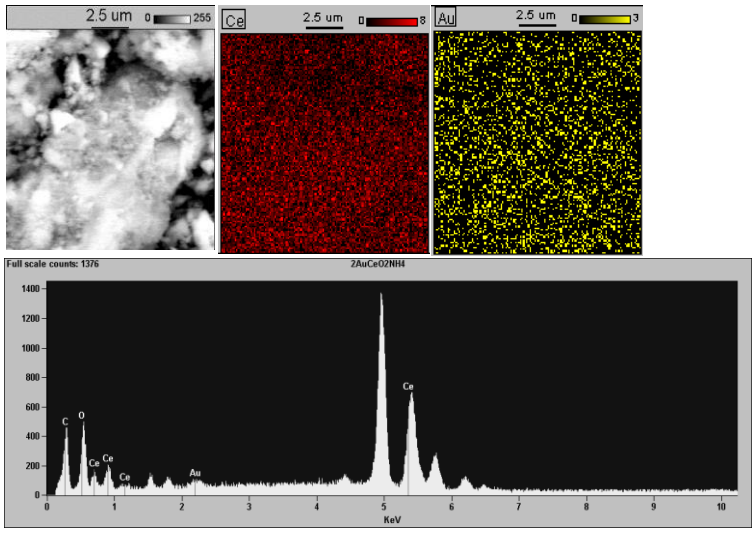


(**b**)

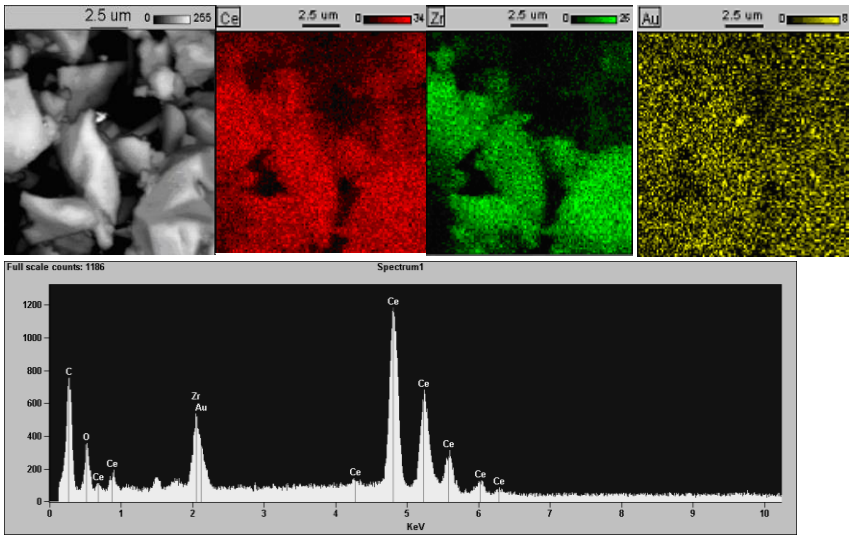


**Figure 5.** *Cont.*

(**c**)

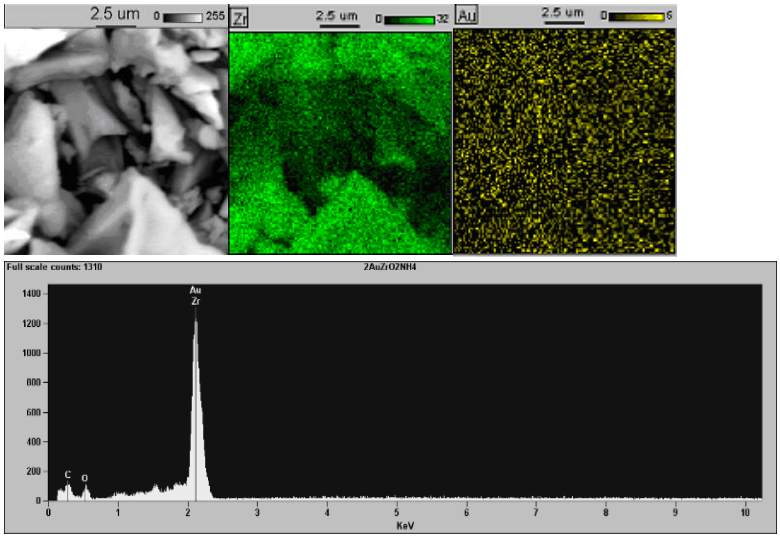


**Figure 5.** The back-scattered electron (BSE) photomicrographs, EDS maps and characteristic X-ray spectra of: (**a**) (2 wt. % Au)/$CeO_2$, (**b**) (2 wt. % Au)/$Ce_{0.75}Zr_{0.25}O_2$ and (**c**) (2 wt. % Au)/$ZrO_2$ catalysts washed with ammonia (copyright permission number 4932711058170) [21].

Figure 6a displays X-ray patterns of $CeO_2$ and (2 wt. % Au)/$CeO_2$ catalysts, prepared without washing and washed with ammonia. Both support and catalysts exhibited four well-pronounced diffraction peaks at 2θ = 28.55°, 33.09°, 47.49° and 56.35°. They correspond to (101) (110) (200) (211) reflections, typical of face-centered cubic (fcc) cell (JCPDS: 03-065-2975) fluorite-type structure. XRD pattern of the catalyst prepared without washing also presents clear Au (111), Au (200) and Au (220) reflections at 2θ = 38.19°, 44.39°, 64.58° (JCPDS: 00-004-0784). The average Au particle size, calculated based on the Scherrer equation using (111) diffraction peak, was 15.0 nm. This result is in agreement with the result of HRTEM ($d_m$ = 15.9 nm) (Figure 3a). For (2 wt. % Au)/$CeO_2$ catalyst prepared without washing, the crystallite size of $CeO_2$, calculated for cerianite (111) plane, equaled to 12.3 nm, similar to that of the unsupported ceria (14.2 nm). Notice that for (2 wt. % Au)/$CeO_2$, the observed diffraction peaks of ceria are shifted towards lower 2θ values (Figure 6a). The observed shift is even more pronounced for the catalysts washed with ammonia. We believe that in the presence of well-dispersed Au particles, during the catalyst calcination process, the autoreduction of $CeO_2$-containing catalysts can take place. This involves the reduction of $Ce^{4+}$ to $Ce^{3+}$, which provokes lattice expansion due to a bigger radius of $Ce^{4+}$ cation (1.14 Å vs. 0.97 Å) [20]. This is also probably the reason for the observed change in catalysts color; in the drying process from yellow to dark gray and in the calcination from dark gray to graphite color. The (2 wt. % Au)/$CeO_2$ catalyst, washed with ammonia, presents the crystallite size of $CeO_2$, calculated for cerianite (111) plane, of 6.4 nm, ca. twice lower than that calculated for the catalyst prepared without washing. Finally, for the catalyst washed with ammonia, Au (111), Au (220) and Au (220) reflections were not found.

XRD patterns of $Ce_{1-x}Zr_xO_2$ (x = 0, 0.25, 0.5, 0.75, 1) and of the series of (2 wt. % Au)/$Ce_{1-x}Zr_xO_2$ catalysts washed with ammonia, is presented in Figure 6b. Similar to the $CeO_2$ system, $Ce_{0.75}Zr_{0.25}O_2$ and (2 wt. % Au)/$Ce_{0.75}Zr_{0.25}O_2$ presents the cubic phase (JCPDS: 00-028-0271). However, for $Ce_{0.5}Zr_{0.55}O_2$, $Ce_{0.25}Zr_{0.75}O_2$, (2 wt. % Au)/$Ce_{0.5}Zr_{0.5}O_2$ and (2 wt. % Au)/$Ce_{0.25}Zr_{0.75}O_2$, tetragonal phase was preferential (JCPDS: 00-038-1436). Simultaneously, comparing to $CeO_2$, for $Ce_{1-x}Zr_xO_2$ (x = 0.25, 0.5, 0.75), the increasing amount of $ZrO_2$ introduced into $CeO_2$ lattice provokes: (i) a slight shift of the main diffraction peaks into higher 2θ values. This is a consequence of the substitution of $Ce^{4+}$ cation ($Ce^{4+}$ cation radius 0.97 Å) with the smaller $Zr^{4+}$ one ($Zr^{4+}$ cation radius 0.84 Å), causing lowering of cell symmetry. The decrease in unit cell parameters was also observed [24]; (ii) a broadening of the main diffraction peaks. This is attributed to the distortion of $CeO_2$ cell, resulting in the decrease in the average crystallites size, as follows: for $Ce_{0.75}Zr_{0.25}O_2$, for cerianite (111) plane,

of 7.0 nm; for $Ce_{0.5}Zr_{0.55}O_2$ and $Ce_{0.25}Zr_{0.75}O_2$, for (101) plane, of 6.4 nm and 6.7 nm, respectively. For all $Ce_{1-x}Zr_xO_2$ no phase segregation was detected, confirming the successful incorporation of $ZrO_2$ into $CeO_2$ lattice and formation of a solid solution. No clear Au reflections were observed for (2 wt % Au)/$Ce_{1-x}Zr_xO_2$ catalysts washed with ammonia, confirming the presence of well-dispersed Au particles (ca. 4 nm, according to HRTEM, Figure 3c). Notice that, similarly to (2 wt. % Au)/$CeO_2$ (Figure 6a), for (2 wt. % Au)/$Ce_{1-x}Zr_xO_2$ (x = 0.25, 0.5, 0.75), a characteristic shift of main diffraction peaks towards lower 2θ values (Figure 6b) is also observed. The following values of crystallite size of catalysts were determined: for (2 wt. % Au)/$Ce_{0.75}Zr_{0.25}O_2$ of 7.2 nm, calculated for cerianite (111) plane, for (2 wt. % Au)/$Ce_{0.5}Zr_{0.5}O_2$ and (2 wt. % Au)/$Ce_{0.25}Zr_{0.75}O_2$ of 6.7 nm and 7.0 nm, respectively, calculated for (101) plane. For $ZrO_2$, both monoclinic (JCPDS: 00-037-1484) and tetragonal phase (JCPDS: 00-050-1089) was identified. The average crystallites size of 23.4 nm, for baddeleyite (−111) plane, and of 19 nm, for (101) plane, was calculated. For (2 wt. % Au)/$ZrO_2$, the average crystallites size of 27.8 nm and 18.8 nm was determined for (−111) and (101) plane, respectively. Moreover, any typical Au reflections were found. Thus, in accordance with HRTEM results (Figure 3c, $d_m$ = 5.6 nm), the presence of well-dispersed and small Au particles can be assumed.

It is well established that the oxidation of CO is affected by the size of the gold crystal, and, in general, the degree of CO oxidation increases with the reduction of the crystal size up to a certain size limit. Below this critical value, CO oxidation decreases (e.g., for Au/$TiO_2$ catalyst, the reported critical value corresponds to 3.8 nm [5]). By decreasing the crystal size of Au to less than 10 nm, Haruta et coworkers found that Au oxidized CO well below 0 °C [6]. In spite of the enhancement of the catalytic activity with crystal size decreasing, this size-dependency is also representing a huge challenge in the use of catalysts with metallic nanoparticles. At the nanoscale, melting point depression occurs to the particles, increasing the mobility of metal atoms over the support surface and increasing the probability of sintering and Ostwald ripening [54]. The size of the catalyst crystals changes the contact limit between the catalyst and the support, which is considered one of the most critical factors in the oxidation of CO. The variation in the catalytic activity has been attributed to various molecular scale factors, including change of surface structure, electronic state, metal-support interactions, an active surface oxide layer (capping oxygen mobility), oxidation states, quantum confinement effects on the nanoparticle electrons, band-gap change also related to quantum effects at the nanoscale size and the increase in unsaturated surface atoms due to the nanoparticle geometry [55].

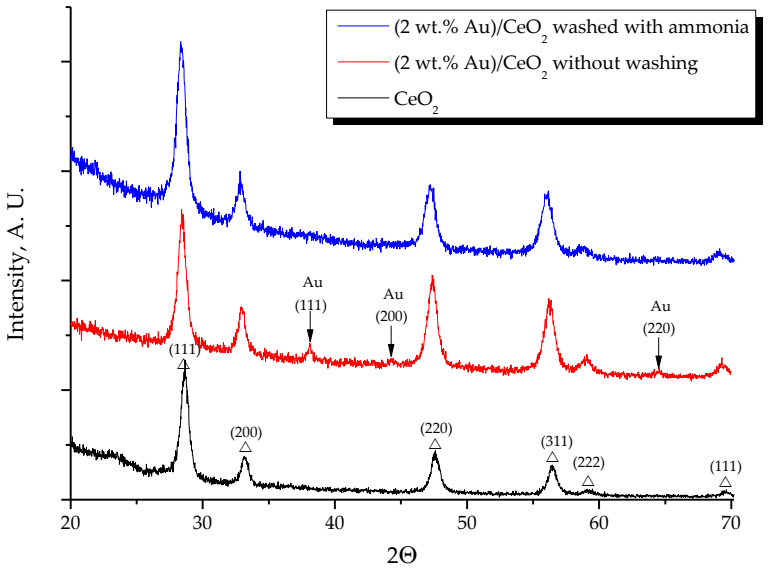


(**a**)

**Figure 6.** *Cont.*

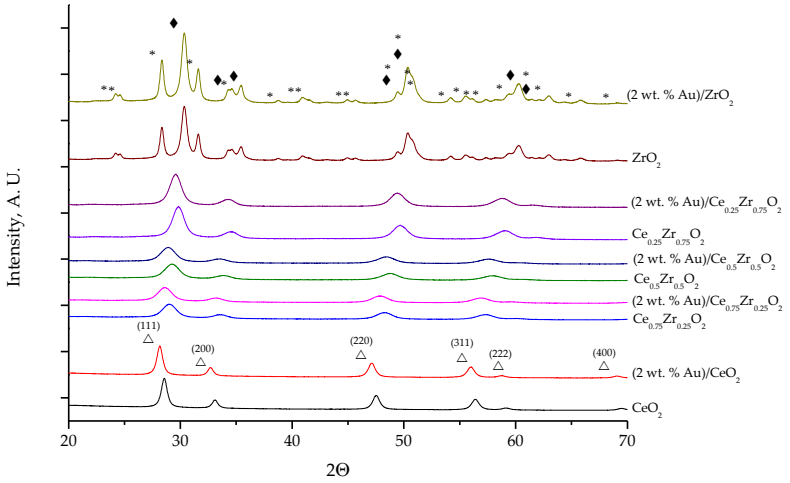


(**b**)

**Figure 6.** X-ray diffraction patterns of (**a**) support ($CeO_2$) and (2 wt. % Au)/$CeO_2$ prepared without washing and washed with ammonia; (**b**) supports ($Ce_{1-x}Zr_xO_2$) and (2 wt. % Au)/$Ce_{1-x}Zr_xO_2$ catalysts washed with ammonia; (Δ) fluorite-type structure (cubic) of $CeO_2$, (*) monoclinic-type structure of $ZrO_2$, (♦) tetragonal-type structure of $ZrO_2$.

Figure 7 presents the effect of the washing procedure on the performance of (2 wt. % Au)/$Ce_{1-x}Zr_xO_2$ catalysts in CO oxidation.

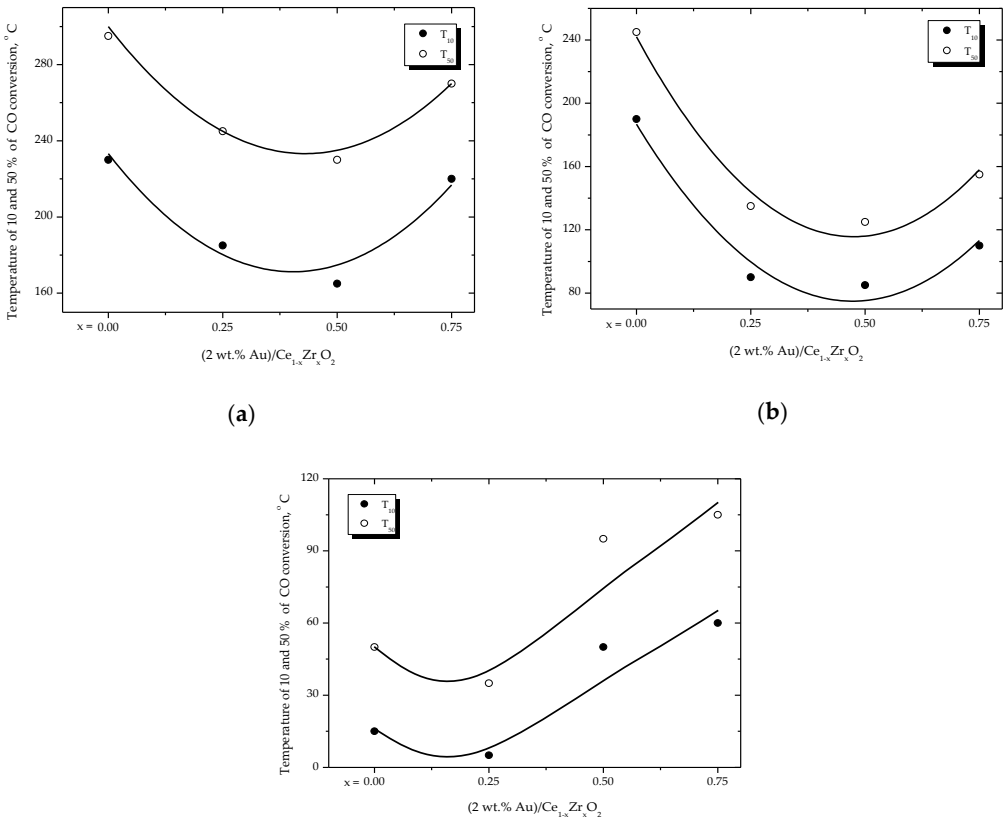


(**a**) (**b**)

(**c**)

**Figure 7.** The effect of the washing procedure on CO oxidation activity of (2 wt. % Au)/$Ce_{1-x}Zr_xO_2$ catalysts: (**a**) prepared without washing; (**b**) washed with warm water; (**c**) washed with ammonia.

For all catalysts prepared without washing, even if they present similar real gold-loading (Figure 1), significant differences in CO oxidation were observed. The (2 wt. % Au)/$Ce_{0.5}Zr_{0.5}O_2$ catalyst presented the highest activity (e.g., the reaction starts at ca. 165 °C). Catalyst washing, with warm water or with ammonia, decreased Au particle size (as shown in Figure 1) and increased the catalytic activity. In comparison with catalysts prepared without washing, catalysts washed with warm water oxidized CO at lower temperatures (ca. 80 °C for the most active one). Moreover, the catalysts washed with ammonia presented a more remarkable decrease in temperature of 10% and 50% CO conversion. The highest activity was observed for (2 wt. % Au)/$Ce_{0.75}Zr_{0.25}O_2$, below room temperature (e.g., 10% conversion was detected at 5 °C). Notice that for this catalyst, ToF-SIMS studies confirmed the presence of $AuCl^-$, $AuClO^-$ and $AuCl_2{}^-$ ions in the surroundings of Au particles (Figure 4), even if residual chloride concentration was lower than 200 ppm. This suggests that high CO conversion on (2 wt. % Au)/$Ce_{1-x}Zr_xO_2$ can be reached even if residual chloride ions are still present in the catalyst. Jóźwiak et al. [56] have found that Au(K)/$Fe_2O_3$ catalyst, with a Cl/Au = 4 ratio, showed considerable activity. However, the increase in the Cl/Au ratio up to 8 led to the catalyst deactivation.

Resuming, the catalytic performance of (2 wt. % Au)/$Ce_{1-x}Zr_xO_2$ depends on (i) Au particle size; (ii) Au dispersion, (ii) residual chloride content; (iv) catalyst´s surface composition and (v) support composition and properties. This last one is discussed below.

### 2.2. *Effect of the Support Composition (Ce/Zr Molar Ratio)*

The effect of support on the catalytic performance of Au catalysts starts since their synthesis. Actually, the selection of preparation procedure is related to the physicochemical properties of the support (e.g., morphology, specific surface area, acid/base properties, presence of surface defects, the possibility of phase transformation, etc.). Both for deposition–precipitation method, developed by Haruta and coworkers [6,7,13] and for the DAE technique, developed by Pitchon and coworkers [17] and used for the preparation of (2 wt. % Au)/$Ce_{1-x}Zr_xO_2$ catalysts [21–24,44–48], a key parameter is the surface charge of the support material. This depends on the pH value of the Au precursor and the isoelectric point (IEP) of the oxide. Their interactions proceed either by anionic or by cation adsorption. The anionic adsorption occurs when the pH of the solution is higher than the IEP of the support (the main surface species is $O^-$; thus, the surface is negatively charged). The cationic adsorption takes place when the pH is lower than the IEP of the support (the main surface species is $OH_2{}^{+,}$ and the support surface is positively charged). Since the IEP of $Ce_{1-x}Zr_xO_2$ is ca. 6.7, and at pH = 2, the dominant species of Au corresponds to the negatively charged ions ($AuCl_x(OH)_{4-x}{}^-$) [57], the anionic exchange of gold species with hydroxyl groups of the support occurs. Anion adsorption (AA) [14], cationic adsorption [58] and co-precipitation [6] methods have also been attempted by many researchers.

Supports can also affect the catalytic properties of supported metallic nanoparticles, and they can play different roles during a reaction. They can provide specific defects where Au nanoparticles can be anchored and/or stabilized. They can let the electron transfer to or from metal particles. They can provide additional functionality (acidity/basicity) to the overall supported metal catalyst. Finally, they can participate in the reaction. Herein, details on the effect of $Ce_{1-x}Zr_xO_2$ composition on catalytic properties of (2 wt. % Au)/$Ce_{1-x}Zr_xO_2$ in CO oxidation are reviewed.

In order to understand the role of support in the creation of catalytic performance of (2 wt. % Au)/$Ce_{1-x}Zr_xO_2$ in CO oxidation, TPR studies were used as a tool. Figure 8 shows TPR-$H_2$ (a) and TPR-CO (b) profiles of $Ce_{0.75}Zr_{0.25}O_2$ and (2 wt. % Au)/$Ce_{0.75}Zr_{0.25}O_2$ catalysts.

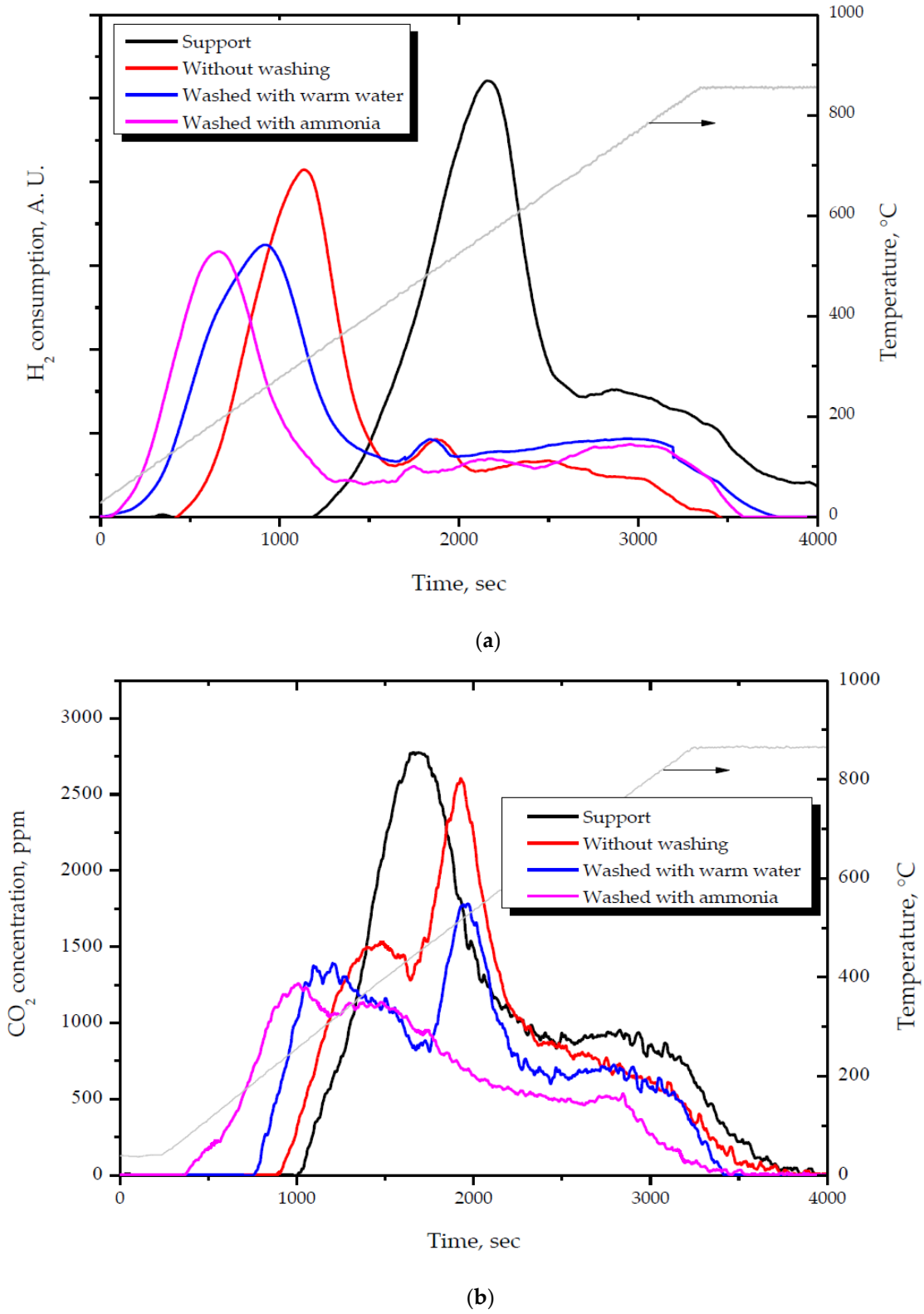


**Figure 8.** Temperature-programmed reduction (TPR-$H_2$) (**a**) and TPR-CO (**b**) profiles of $Ce_{0.75}Zr_{0.25}O_2$ support and (2 wt. % Au)/$Ce_{0.75}Zr_{0.25}O_2$ catalysts.

The reduction of $Ce_{0.75}Zr_{0.25}O_2$ mixed oxide occurs in one stage with the maximum at 565 °C using $H_2$ as a reducing agent. (Figure 8a). For (2 wt. % Au)/$Ce_{0.75}Zr_{0.25}O_2$ catalysts, the characteristic $H_2$ reduction peak is shifted toward a lower temperature in the presence of Au nanoparticles characterized

by different sizes. It is assigned to the co-reduction of $Au^{3+}$ and of surface oxygen. The observed decrease in the reduction temperature, comparing to the unsupported mixed oxide, is related to the activation of $H_2$ molecule on Au nanoparticles followed by the migration of dissociated hydrogen species, by a spillover process, from the surface of the Au particles to the support [44,46]. However, if the catalyst contains only ionic Au, the surface oxygen reducibility could be intensified through the lattice substitution mechanism [3,4]. According to those statements, the $Au^+$ or $Au^{3+}$ ions could fill the vacant $Ce^{4+}$ sites, resulting in oxygen vacancy formations and an increase in oxygen mobility and reducibility. One can see that the smaller the Au particle size is, the bigger the shift of the reduction peak is observed. Moreover, for all (2 wt. % Au)/$Ce_{0.75}Zr_{0.25}O_2$ catalysts, a substantial decrease in TPR-$H_2$ signal intensity is observed. Estimated $H_2$ consumption strongly depends on Au particle size, with the minimum observed for the catalyst washed with ammonia. Considering that the washing procedures removes residual chlorine, which is also known to inhibit the reducibility of Ce-containing oxides, the catalyst autoreduction during calcination occurs [21]. Notice that amount of $H_2$ used for the reduction of dried (uncalcined) (2 wt. % Au)/$Ce_{0.75}Zr_{0.25}O_2$ catalyst, washed with ammonia, was higher (1.12 mmol/g) than that observed for the calcined catalyst, washed with ammonia (0.95 mmol/g). For comparison, the $H_2$ consumption for $Ce_{0.75}Zr_{0.25}O_2$ reduction equaled to 1.53 mmol/g.

When CO is used as a reducing agent, the reduction of $Ce_{0.75}Zr_{0.25}O_2$ mixed oxide occurs in one stage with the maximum at 460 °C (Figure 8b). A characteristic shoulder is also observed at low temperature. This suggests the existence of at least two types of $Ce^{x+}$ located at different chemical environments, assigned to the reduction of surface and subsurface $Ce^{x+}$, susceptible to the reduction at a lower temperature in the presence of Au. Thus, for (2 wt. % Au)/$Ce_{0.75}Zr_{0.25}O_2$ catalysts, the characteristic $CO_2$ formation peak consists of two overlapping peaks indicating two reduction process: (i) the first one related to the reduction of both the oxygen species coordinated around dispersed Au nanoparticles and the surface capping oxygen of support, strongly anchored with Au, and (ii) the second one, corresponding to the reduction of both oxygen species coordinated around larger Au particles and the support surface layers, not strongly anchored with Au. The smaller the Au particle size is, the bigger the shift of the reduction peak is observed. Similar to TPR-$H_2$ profiles, the contribution of low-temperature reduction peak decreases with a decrease in Au particle size, as confirmed by HRTEM results (Figure 3), due to the catalyst autoreduction.

Figure 9 shows the correlation between the hydrogen consumption, the ratio of oxygen atoms in the capping peak to the total cerium atoms and the activity of (2 wt. % Au)/$Ce_{0.75}Zr_{0.25}O_2$ catalysts prepared using different washing procedures. The sequence of the decreasing temperature of CO oxidation indicates that the activity of Ce-containing oxides in CO oxidation depends on the amount of capping oxygen available at the lowest temperature. TPR-$H_2$ studies showed a marked effect of well-dispersed Au nanoparticles and its size on the reducibility of $Ce_{0.75}Zr_{0.25}O_2$ support at low temperatures. For Au catalysts, the $H_2$ consumption for the removal of surface capping oxygen atoms is higher than that for the oxide support. One can see that the sequence of the increasing activity of the studied catalysts follows the increasing percentage of oxygen atoms in the capping peak to the total cerium atoms ($O_c$/Ce) (Figure 9).

These findings indicate the role of both Au particle size and the support redox properties in the creation of the catalytic performance of (2 wt. % Au)/$Ce_{0.75}Zr_{0.25}O_2$ catalysts. The higher reducibility of the oxide support, in the presence of well-dispersed and small Au nanoparticles, increases the concentration of surface oxygen vacancies available at low temperatures. Considering that CO adsorption was observed on both $Au^{3+}$, $Au^+$, $Au^0$ species and $CeO_2$ ($Ce^{4+}$-CO), a synergetic effect between the support and Au nanoparticles at the interface could be implied. However, for $Ce_{0.75}Zr_{0.25}O_2$ oxide, any CO conversion was observed at temperatures below 200 °C. Thus, well-dispersed Au was responsible for the improvement of its catalytic activity.

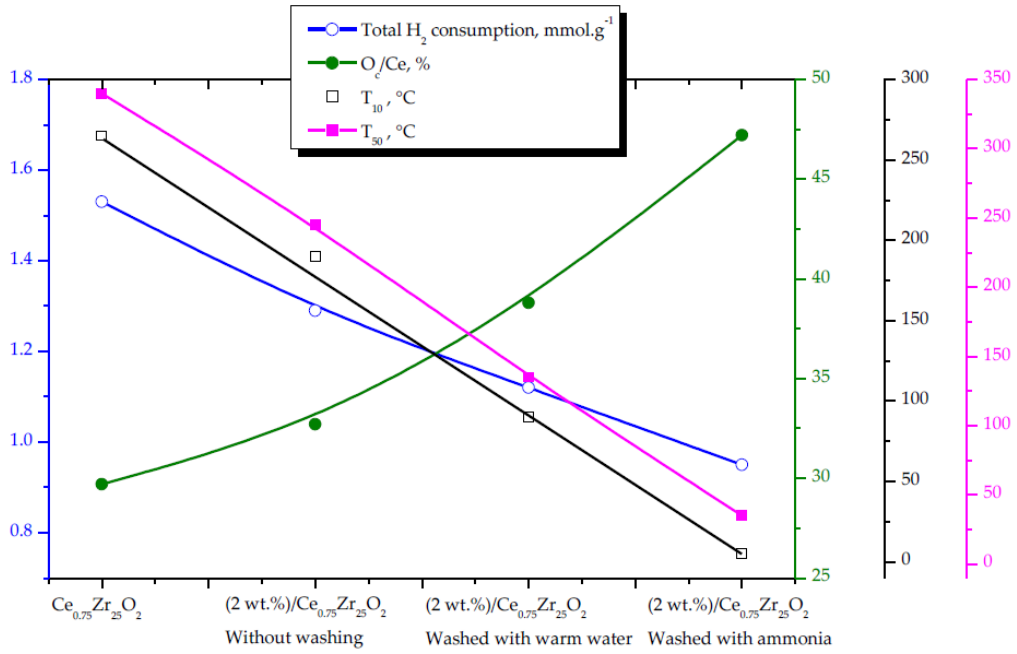


**Figure 9.** The correlation between the hydrogen consumption, the ratio of oxygen atoms in the capping peak to the total cerium atoms and the activity of (2 wt. % Au)/$Ce_{0.75}Zr_{0.25}O_2$ catalysts prepared using different washing procedures.

Although the nature of the active sites and the reaction mechanism is a matter of debate, there is an agreement that the activity in CO oxidation is ruled by the contact boundaries between oxide support and Au nanoparticles. Indeed, the observed differences in CO oxidation activity overstudied catalysts depend on Au particles size and their dispersion (Figure 10), since the smallest nanoparticles enhanced the Au-oxide contact boundaries formation. Notice that (2 wt. % Au)/$ZrO_2$ catalyst presented the lowest activity as well as the biggest particle size of Au and oxide support (Figures 1 and 6b). Consequently, the support particle size and reducibility (which depends on the composition) appear to be crucial in the creation of catalytic performance of supported Au catalysts in CO oxidation.

For unsupported $Ce_{1-x}Zr_xO_2$, the sequence of decreasing temperature of the maximum reduction peak clearly follows the sequence of increasing activity of these oxides in CO oxidation (Figure 10a). Ce-rich oxides ($CeO_2$ and $Ce_{0.75}Zr_{0.25}O_2$) were the most active ones. They were characterized by both a cubic crystalline phase and high reducibility at lower temperatures. Accordingly, the presence of the cubic phase in the Ce-Zr solid solution improves its catalytic activity in CO oxidation [47].

For (2 wt. % Au)/$Ce_{1-x}Zr_xO_2$ catalysts (Figure 10b–d), more homogenously dispersed Au nanoparticles increased the reducibility of the studied oxides, mostly at lower temperatures. Moreover, the initial temperature of the catalyst reduction, using CO as a reducing agent, corresponded to the $T_{50}$. For details see [21,24]. This shows the role of support redox properties, in the presence of well-dispersed Au, in the creation of catalytic activity of (2 wt. % Au)/$Ce_{1-x}Zr_xO_2$ in CO oxidation. Notice that (2 wt. % Au)/$Ce_{0.75}Zr_{0.25}O_2$ was the most active catalyst. It is reducible at the lowest temperature due to a higher concentration of surface oxygen vacancies (which can be the centers of oxygen activation). Such vacancies may be formed even in the reaction mixture CO + $O_2$ exhibiting lower redox potential compared to the oxygen atmosphere, as reported by Grzybowska-Świerkosz [59] and Guzmán et al. [60]. It can be suggested that ceria, which is reducible at the lowest temperatures, appears to be responsible for the activity of these catalysts in CO oxidation.

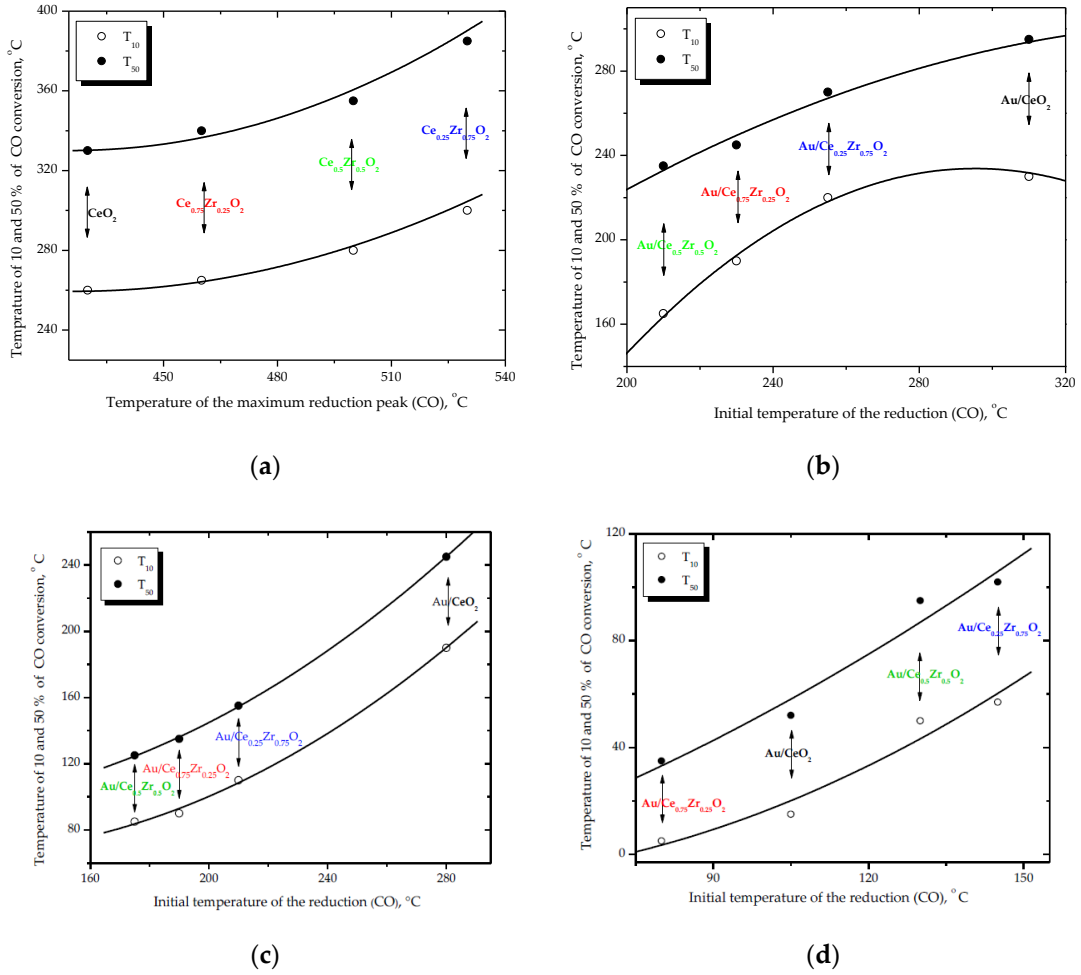


**Figure 10.** The effect of $Ce_{1-x}Zr_xO_2$ composition on the activity of (2 wt. % Au)/$Ce_{1-x}Zr_xO_2$ catalysts in CO oxidation (any activation procedure was used before the activity tests): (**a**) supports (for comparison); (**b**) prepared without washing; (**c**) washed with water; (**d**) washed with ammonia.

### *2.3. Influence of the Pretreatment Atmosphere*

The performance of Au/metal oxide catalysts in CO oxidation can be altered by the pretreatment atmosphere as it directly affects the surface composition of the catalytic system. For example, in the presence of water, an increase in the CO oxidation activity for Au supported on $TiO_2$, $Fe_2O_3$, $Al_2O_3$, $Mg(OH)_2$ was reported [61]. However, Olea et al. [62] informed that in the presence of water, the catalytic activity of $Au/TiO_2$ decreases. Thus, due to the relevance on the practical applications, we studied the effect of pretreatment atmosphere (e.g., dry He, air, $H_2$ and $H_2$ + water, realized at 200 °C) on CO conversion at 30 °C on (2 wt. % Au)/$Ce_{1-x}Zr_xO_2$ catalysts washed with ammonia (Figure 11) [45].

The thermal treatment of all (2 wt. % Au)/$Ce_{1-x}Zr_xO_2$ in dry He significantly decreases their catalytic activity (ca. 50%) in relation to the calcined catalysts (Figure 11). However, the observed decrease in activity was re-established, exposing the catalysts, at room temperature, to the stream of moisture (6000 ppm)/He. We believe that the loss of hydroxyl species from the catalyst surface is the reason for the observed deactivation. A similar observation was also reported by Costello et al. [63]. The activity of the dried (as prepared) (2 wt. % Au)/$Ce_{1-x}Zr_xO_2$ catalysts was significantly higher than that of the calcined ones (Figure 11). Notice that the dried systems were not pretreated before activity testing. This implies that high CO oxidation yields require the presence of water-derived species on the (2 wt. % Au)/$Ce_{1-x}Zr_xO_2$ surface. Thus, the moisture adsorbed on the catalyst surface is responsible for the creation of catalytic performance rather than its content in the feed stream. However, their activity was unsteady in time and catalysts deactivation after 30 min of reaction took

place. It was just partially re-established, exposing the catalysts, at room temperature, to the stream of moisture (6000 ppm)/He. The pretreatment in the $H_2$ stream, at 200 °C, of (2 wt. % Au)/$CeO_2$ and (2 wt. % Au)/$Ce_{0.75}Zr_{0.25}O_2$ catalysts significantly increased their catalytic activity in comparison with the calcined samples. Notice that the activity of the pre-reduced catalyst was steady in time. Any deactivation was observed after a few hours of reaction. This suggests that rather the reduction of Au nanoparticles, instead of support reduction, is responsible for the increase in activity observed over pre-reduced contacts [64]. Moreover, the pre-reduced systems showed better performance in CO oxidation than the unreduced ones. Thus, both metallic (Au°) and oxidized ($Au^{x+}$) species are needed for high CO conversion at low temperatures [65,66]. On the other hand, the increase in the reduction temperature ($H_2$ stream, at 290 °C), which allowed obtaining a higher amount of metallic Au°, provoked the decrease in activity [45]. This indicates that partial reduction of $Au^{3+}$ to Au° favors high CO oxidation yields. In this case, it was achieved by reducing the catalysts at lower temperatures ($H_2$ treatment at 200 °C). Finally, the catalyst pretreatment in an oxidative atmosphere (air) decreases catalytic activity. This probably due to the increase in the amount of $Au^{3+}$ species. For (2 wt. % Au)/$ZrO_2$, independent of the treatment atmosphere, no CO conversion was observed at low temperature.

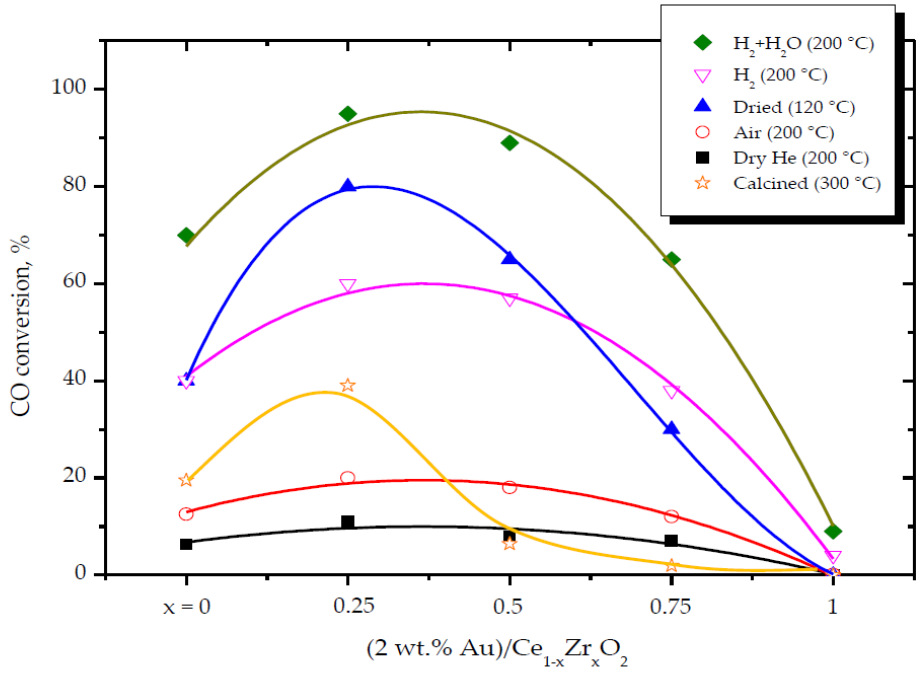


**Figure 11.** The influence of the pretreatment atmosphere on CO conversion at 30 °C on (2 wt. % Au)/$Ce_{1-x}Zr_xO_2$ catalysts washed with ammonia ($CO:O_2$:He = 1.7:3.4:balance; W/F = 0.12 g s $cm^{-3}$).

The $H_2$-TPR profiles of (2 wt. % Au)/$Ce_{0.75}Zr_{0.25}O_2$ catalyst, washed with ammonia, pretreated in different atmospheres, are presented in (Figure 12). One can see that the reduction of each catalyst occurs in one stage. The observed reduction peak is assigned to the co-reduction of $Au^{3+}$ and surface oxygen on $Ce_{0.75}Zr_{0.25}O_2$. In the presence of Au, the reducibility of the $Ce_{0.75}Zr_{0.25}O_2$ surface oxygen is improved, and it facilitates the oxygen transfer across the solid–gas interface during the reaction. The pretreatment in different atmospheres shifts the characteristic reduction peak to the lower temperature in the following sequence: $H_2$ + $H_2O$ (168 °C) < dry air (175 °C) ≈$H_2$ (177 °C) < He (185 °C) < calcined (190 °C) ≈dried catalyst (190 °C).

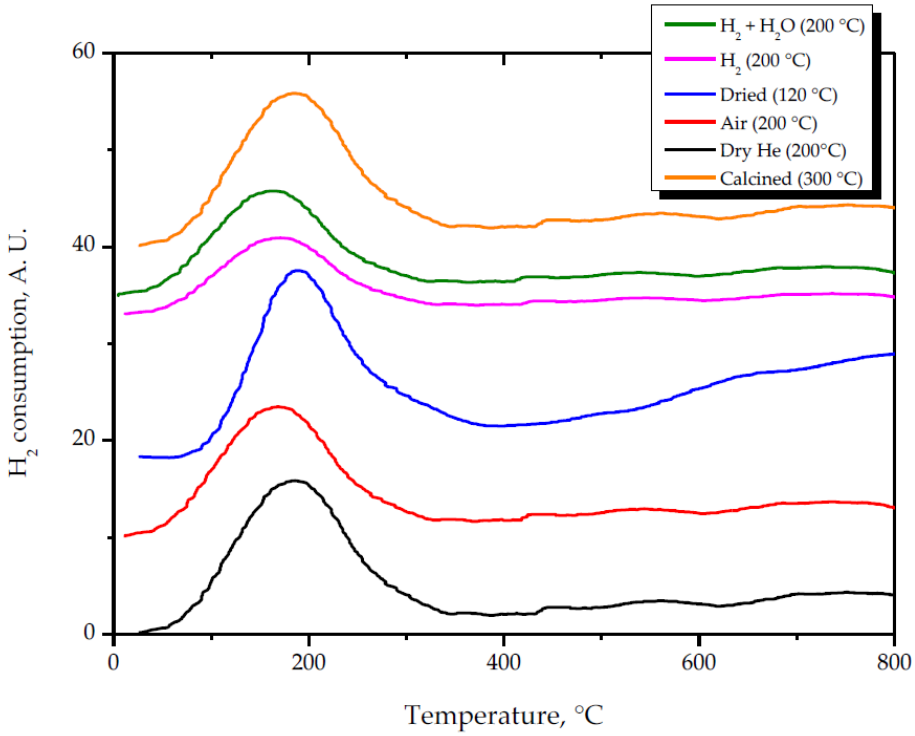


**Figure 12.** The effect of the pretreatment atmosphere on the reducibility of (2 wt. % Au)/$Ce_{0.75}Zr_{0.25}O_2$ catalyst washed with ammonia.

Moreover, a significant difference in the total $H_2$ consumption needed for the catalyst reduction was observed. For the catalyst treated with dry He, the $H_2$ consumption (0.93 mmol/g) is very similar to that of the calcined sample (0.95 mmol/g). This indicates that this treatment can only remove the surface impurities from (2 wt. % Au)/$Ce_{0.75}Zr_{0.25}O_2$ catalyst surface. For the as-prepared (dried) catalyst, the highest value of $H_2$ consumption was observed (1.12 mmol/g). This suggests that the dried catalyst contains mostly $Au^{3+}$ and probably does not possess $Au^0$. For the catalyst pretreated in air, $H_2$ consumption equaled 0.99 mmol/g, indicating the presence of a considerable amount of $Au^{x+}$ on the catalyst surface. The catalyst pretreated in $H_2$ possesses a significantly higher amount of $Au^0$ on the surface ($H_2$ consumption 0.57 mmol/g was registered). Finally, the lowest amount of $H_2$ (0.49 mmol/g) was used for the reduction of the most active catalyst after pretreatment in the $H_2 + H_2O$ stream. Thus, the following observations with respect to observed activity can be made: (i) Two active forms of Au can be responsible for high activity in CO oxidation: $Au^0$ and $Au^{3+}$. The $Au^0$ is crucial for CO adsorption. The $Au^{3+}$ species, in conjunction with $Au^0$, are essential for the activation of surface hydroxyl groups. Next, the activated OH groups can react with the adsorbed CO to form carboxylate species [8,9,53,65,66]. However, a high amount of $Au^{x+}$ or Au° decreases the activity. In fact, the appropriate ratio of $Au^{x+}$ and Au° is critical to obtain the highest catalytic activity in CO oxidation [67–69]; (ii) The adsorption and activation of $O_2$ take place on the support oxygen vacancies. During CO oxidation at oxygen lean conditions, Ce-containing catalysts worked as oxygen buffers by release–uptake of oxygen [21]. (iii) In the presence of moisture, the $O_2$ molecules can dissociate easier and can rapidly react with adsorbed CO [45]. Moreover, Au electronic state can be modified; (iv) High CO oxidation yields, on (2 wt. % Au)/$Ce_{1-x}Zr_xO_2$, require the presence of water-derived species on the catalyst surface. Thus, the moisture adsorbed on the catalyst surface, rather than its content in the feed stream, is responsible for the creation of the catalytic performance.

The obtained results suggest that CO oxidation under stationary conditions over Ce-containing oxides occurs by the Au-assisted Mars van Krevelen (MvK) redox-type mechanism. It consists of: (i) the metal/support oxidation in separate and independent steps, (ii) adsorption of CO from the gas phase on

the oxide, (iii) reaction between the adsorbed CO and catalyst surface oxygen, accompanied with the creation of oxygen vacancies, (iv) $CO_2$ desorption from the catalyst surface and (v) fast and irreversible refilling of the resulting oxygen vacancies by oxygen from the gas phase, in a separate step (as in i). The MvK model is able to predict CO oxidation experimental data at stoichiometric and rich conditions, even if some of them present a very fast increase in conversion with the reaction temperature [48]. Consequently, the principal role of Au in CO oxidation over (2 wt % Au)/$Ce_{1-x}Zr_xO_2$ catalysts could be related to the promotion in the transformation process of reversibly adsorbed or inactive surface oxygen into irreversibly adsorbed species, active in CO oxidation. On the other hand, according to the reactivity results, Figure 7, the highest quantity of oxygen that can be involved in the reaction, must be available at the same temperatures at which CO oxidation occurs. It suggests that the reaction involves both gas-phase oxygen and surface—bulk oxygen, indicating the ability of Ce-containing oxides to supply reactive oxygen to Au active species for CO oxidation. It supports the idea of Ce acting as an oxygen buffer by releasing-up taking oxygen through the redox processes involving $Ce^{4+}/Ce^{3+}$ redox couple. Similar observations were reported elsewhere [70–72]. Additional experiments performed under totally anaerobic conditions (without oxygen present in the gas phase), showing that the catalyst activity depends on its ability to release first the surface and then bulk oxygen [48]. Thus, as expected, the most active catalyst is (2 wt. % Au)/$Ce_{0.75}Zr_{0.25}O_2$, which presents the highest oxygen mobility (Figure 9).

## 3. Materials and Methods

### *3.1. Synthesis of Catalysts*

A series of $Ce_{1-x}Zr_xO_2$ (x = 0.25, 0.5, 0.75) solid solutions, $CeO_2$ and $ZrO_2$ used as a support for Au was prepared by the sol–gel-like method, based on thermal decomposition of mixed propionates [73]. The starting materials, zirconium (IV) acetylacetonate ($Zr(CH_3COCH_2COCH_3)_4$, purity 99.9%, Avocado, Tewksbury, MA, USA) and/or cerium (III) acetyloacetonatehydrate ($Ce(CH_3COCH_2COCH_3)_3$ $H_2O$, purity 99.9%, Sigma–Aldrich, St. Louis, MO, USA) and calcined at 550 °C, in details described previously [21].

(2 wt. % Au)/$Ce_{01-x}Zr_xO_2$ catalysts were prepared by the direct anionic exchange (DAE) method of Au species with hydroxyl groups of support, based on a previously established procedure [21,23]. In brief, hydrogen tetrachloroaureate (III) trihydrate ($HAuCl_4.3H_2O$, purity 99.9%, Sigma–Aldrich, St. Louis, MO, USA) was used as a gold precursor. The catalysts were prepared by the direct anionic exchange (DAE) method of gold species with hydroxyl groups of the support. The optimization of catalyst synthesis conditions was presented previously [24]. An aqueous solution of $HAuCl_4$ at the concentration of $2.25 \times 10^{-4}$ M was prepared using 900 $cm^3$ of distilled water. The solution was heated up to 70 °C, and the support was introduced. After 1 h of thermostatting and vigorous stirring, the suspension was centrifuged. In order to remove the residual chlorine from the catalysts, two washing procedures prior to the drying process were applied. Depending on the washing procedure, the solids were suspended in either 4 M ammonia solution at 25 °C or deionized water at 50 °C and stirred for 1 h and next centrifuged again. After drying in an oven at 120 °C overnight ((2 wt. % Au)/$Ce_{1-x}Zr_xO_2$ dried or as prepared), the catalysts were calcined in air at 300 °C ((2 wt. % Au)/$Ce_{1-x}Zr_xO_2$ calcined) for 4 h.

### *3.2. Characterization Methods*

The specific surface area was determined by BET method using a Sorptomatic 1900 apparatus (Carlo-Erba, Milan, Italy) with $N_2$ as an adsorbate. Prior to the measurement, all samples were degassed for 4 h at 250 °C.

The morphology of the prepared catalytic systems was studied using a-4700 scanning electron microscope, SEM (HITACHI, Tokyo, Japan), equipped with an energy-dispersive spectrometer,

EDS (ThermoNoran, Madison, WI, USA). Before analyzing, the samples were coated with a carbon monolayer in order to reduce the charge buildup on the surface.

The amount of Au deposited on $Ce_{0.75}Zr_{0.25}O_2$ was determined using an atomic absorption spectroscope (AAS), specifically a Solaar M6 Unicam spectrophotometer. Prior to the analysis, each sample was digested by aqua regia (3 $cm^3$ + 100 mg of the sample), using a microwave oven (MLS-1200 MEGA, Milestone, Apeldoorn, The Netherlands), and the resulting solution was diluted with 100 $cm^3$ of deionized water. A blank test was prepared in a similar way.

High-resolution transmission electron microscopy (HRTEM) measurements were carried out using high-resolution microscope EM-002B (TOPCON, Tokyo, Japan), at an acceleration voltage 200 kV, equipped with an energy-dispersive spectrometer (EDS). To determine an average Au particle size and to define their distribution more accurately, at least 500 particles of each catalyst were chosen. The mean particle diameters were calculated, as described previously [18].

X-ray diffraction patterns were obtained at room temperature using a PANalytical X'Pert Pro MPD diffractometer (Malvern, UK), operating at 40 kV and 30 mA (Cu Ka radiation). Data were collected in the range 20–70° 2θ, with a step size of 0.01678 and a step time of 10 s. JCPDS files were used for the identification of the diffraction peaks. Approximately 300 mg of sample, which had been hand ground in an agate mortar, was packed in the sample holder. The particle size was estimated from the width of principal diffraction peaks using the Scherrer equation.

Time-of-flight secondary ion mass spectrometry (ToF–SIMS) was applied to determine the chemical state of gold in the catalysts. The measurements were performed using the ION-TOF GmbH instrument (TOF–SIMS IV, Münster, Germany) equipped with 25 kV pulsed $^{69}Ga^+$ primary ion gun in the static mode. The analyzed area corresponded to a square of 500 μm × 500 μm. Before the measurements, the samples were pressed into pellets and attached to the sample holder using a double-sided tape. Moreover, a pulsed electron flood gun was used for charge compensation. Thus, the peak with *m*/*z* of 197 was assigned to Au. The peaks with m/z of 213, 214, 229, 232, 248 and 267 were ascribed to ion fragments of $AuO^-$, $AuOH^-$, $AuO_2^-$, $AuCl^-$, $AuClO^-$ and $AuCl_2^-$, respectively.

Temperature-programmed reduction (TPR-CO) measurements were carried out using the PEAK-4 apparatus, using CO as a reducing agent. The apparatus was equipped with an infrared gas analyzer (type: ZRJ-4, Fuji Electric Systems Co., Tokyo, Japan) to analyze $CO_2$ formation. TPR-CO experiments were performed using a CO/He (5 vol % CO, 95 vol % He) gas mixture, with a flow rate of 40 $cm^3$/min, in the temperature range 25–850 °C, with a ramp rate 15 °C/min. Powdered samples of 100 mg were exposed to dry Ar at 250 °C for 1 h before the reduction. Based on the $CO_2$ formation, reduction degrees of the investigated samples were calculated as described previously in detail [21].

Temperature-programmed Reduction (TPR-$H_2$) experiments were carried out using the PEAK-4 apparatus equipped with a thermal conductivity detector (TCD). They were performed using an $H_2$/He (5 vol % $H_2$, 95 vol % He) gas mixture, with a flow rate of 40 $cm^3$/min, in the temperature range 25–850 °C, with a ramp rate 15 °C/min. Powdered samples of 100 mg were exposed to dry Ar at 250 °C for 1 h before reduction.

CO oxidation reaction was carried out at atmospheric pressure in a quartz flow microreactor containing 100 mg of sample in a fixed bed, using a series of mass flow controllers with diluted gases.

Prior to the catalytic tests, the samples were heated in the gas mixture stream at 300 °C for 1 h with a ramp rate of 5 °C/min, except for the pretreatment studies. In these last case, the catalysts were pretreated at 200 °C for 60 min in different atmospheres including: air (99.9 vol % Air), dry He (99.9 vol % He), $H_2$ (5 vol % $H_2$, 95 vol % Ar), $H_2$ + $H_2O$ (5.0 vol %)/$H_2O$ (0.1 vol %)/Ar (94.9 vol %). The gas mixture containing 1.7 vol % CO and 3.4 vol % $O_2$ (He as an eluent gas) was used for CO oxidation tests (flow rate of 50 $cm^3$/min.). The activity tests were performed either in the temperature range of 25–300 °C, with a ramp rate of 5 °C/min or at isothermal conditions (at 30 °C). They were repeated several times in order to verify reproducibility. CO and $O_2$ concentrations were analyzed using a gas chromatograph fitted with molecular sieves 5 Å and equipped with a thermal conductivity detector. CO conversion was calculated, as described previously [21]. The catalytic performance of

studied materials was assessed in terms of both $T_{10}$ and $T_{50}$ temperatures, defined as the temperature at which 10% and 50% conversion was obtained, respectively.

The model developed by Johnson and Mooi [74,75] is based on the qualitative relationship between the magnitude of the capping oxygen and BET surface area. For this model, the authors considered that the reduction of $CeO_2$ corresponds to the elimination of one-fourth of the surface oxygen ions and that each ceria crystallite is the cube of n oxygen ions on a side. Therefore, each ceria crystallite contains $n^3$ oxygen ions and $\frac{1}{2}n^3$ Ce ions. Since the number of capping oxygen ions in a crystallite is: $O_c = n^3 - (n-2)^3 = 6n^2 - 12n + 8$ and the number of H atoms to reduce half of the $O_c$ ions is: $H_c = 2 \cdot O_c$, the ratio of hydrogen atoms in the capping peak to the total cerium atoms ($H_c$/Ce) will be: $H_c/Ce = 4(6n^2 - 12n + 8)/n^3$.

## 4. Conclusions

The most important achievements and conclusions arising from the own authorship contributions concerning (2 wt. % Au)/$Ce_{1-x}Zr_xO_2$ catalyst's active sites in low-temperature CO oxidation were reviewed. They can be summarized as follows:

- High activity of (2 wt. % Au)/$Ce_{1-x}Zr_xO_2$ catalysts in low-temperature CO oxidation is displayed by Au nanoparticles with an optimum size of ca. 4 nm. In the presence of residual chlorine, Au agglomeration during the calcination process occurs. Washing of the catalysts with ammonia effectively prevents Au sintering. The smallest Au nanoparticles and the highest activity in CO oxidation presented catalysts washed with ammonia.
- The electronic properties of nanosized Au can be modified by the oxide support. The structure and properties of oxide support define the nature of Au-support interactions. High oxygen mobility at low temperatures is critical for high activity. The catalytic performance of (2 wt. % Au)/$Ce_{1-x}Zr_xO_2$ contacts strongly depends on the support's redox properties. Oxygen vacancies on the support surface are centers for oxygen molecule activation.
- Concerning Au active species: (i) Two active forms of Au can be responsible for high activity in CO oxidation: $Au^0$ and $Au^{3+}$. The $Au^0$ is crucial for CO adsorption. The $Au^{3+}$ species, in conjunction with $Au^0$, are essential for the activation of surface hydroxyl groups. Next, the activated OH groups can react with the adsorbed CO to form carboxylate species. However, a high amount of $Au^{x+}$ or Au° decreases the activity. In fact, the appropriate ratio of $Au^{x+}$ and Au° is critical to obtain the highest catalytic activity in CO oxidation; (ii) The adsorption and activation of $O_2$ take place on the support oxygen vacancies; (iii) The moisture can both enhance the dissociation of $O_2$ molecules adsorbed on the oxygen vacancies and modify the electronic state of gold. Next, the activated oxygen can rapidly react with CO adsorbed on the metallic $Au^0$; (iv) High CO oxidation yields require the presence of water-derived species on the catalyst surface. Thus, the moisture adsorbed on the catalyst surface, rather than its content in the feed stream, is responsible for the creation of the catalytic performance.
- Regarding the reaction mechanism: The Au-assisted MvK model was suggested as more relevant to describe the kinetics of CO oxidation over $Ce_{1-x}Zr_xO_2$ and (2 wt. % Au)/$Ce_{1-x}Zr_xO_2$ catalysts. Consequently, the principal role of Au in CO oxidation over (2 wt. % Au)/$Ce_{1-x}Zr_xO_2$ catalysts can be related to the promotion in the transformation process of reversibly adsorbed or inactive surface oxygen into irreversibly adsorbed species active in CO oxidation. Additionally, at oxygen-lean conditions, the activity seems to be dependent on the ability of the oxide to release first the surface and then bulk oxygen. Thus, considering that extra oxygen is available from the catalyst surface bulk, it was possible to properly fit the observed catalyst activity. Finally, the proposed fitting procedure, based on MvK expression, can be considered as successful for all conditions tested for the CO oxidation reaction.

**Author Contributions:** Conceptualization: I.D.-G.; methodology: I.D.-G.; software, I.D.-G. and M.-Á.G.-G.; formal analysis: I.D.-G.; investigation: I.D.-G.; resources: I.D.-G., J.M.R.; writing—original draft preparation: I.D.-G.; writing—review and editing: I.D.-G., M.-Á.G.-G. and J.M.R. All authors have read and agreed to the published version of the manuscript.

**Funding:** This research received no external funding.

**Conflicts of Interest:** The authors declare no conflict of interest.

## References

1. Lykaki, M.; Stefa, S.; Carabineiro, S.A.C.; Pandis, P.K.; Stathopoulos, V.N.; Konsolakis, M. Facet-Dependent Reactivity of $Fe_2O_3/CeO_2$ Nanocomposites: Effect of Ceria Morphology on CO Oxidation. *Catalysts* **2019**, *9*, 371. [CrossRef]
2. Soliman, N.K. Factors Affecting CO Oxidation Reaction over Nanosized Materials: A Review. *J. Mater. Res. Technol.* **2019**, *8*, 2395–2407. [CrossRef]
3. Bond, G.C.; Thompson, D.T. Gold-catalyzed oxidation of carbon monoxide. *Cat. Rev. Sci. Eng.* **1999**, *41*, 319. [CrossRef]
4. Hashmi, A.S.K.; Hutchings, G.J. Gold Catalysis. *Angew. Chem. Int. Ed.* **2006**, *45*, 7896–7937. [CrossRef]
5. Du, M.; Sun, D.; Yang, H.; Huang, J.; Jing, X.; Odoom-Wubah, T.; Wang, H.; Jia, L.; Li, Q. Influence of Au particle size on $Au/TiO_2$ catalysts for CO oxidation. *J. Phys. Chem. C* **2014**, *118*, 19150–19157. [CrossRef]
6. Haruta, M.; Yamada, N.; Kobayashi, T.; Iijima, S. Gold catalysts prepared of coprecipitation for low-temperature oxidation of hydrogen and carbon monoxide. *J. Catal.* **1989**, *115*, 301–309. [CrossRef]
7. Haruta, M.; Date, M. Advances in the catalysis of Au nanoparticles. *Appl. Catal. A Gen.* **2001**, *222*, 427–437. [CrossRef]
8. Zhou, A.; Wang, J.; Wang, H.; Li, H.; Wang, J.; Shen, M. Effect of active oxygen on the performance of $Pt/CeO_2$ catalysts for CO oxidation. *J. Rare Earths.* **2018**, *36*, 257–264. [CrossRef]
9. Haruta, M. Size- and Support-Dependency in the Catalysis of Gold. *Catal. Today* **1996**, *36*, 153–166. [CrossRef]
10. Cui, Y.; Xu, L.; Chen, M.; Lv, C.; Lian, X.; Wu, C.; Yang, B.; Miao, Z.; Wang, F.; Hu, X. CO Oxidation over Metal Oxide ($La_2O_3$, $Fe_2O_3$, $PrO_2$, $Sm_2O_3$, and $MnO_2$) Doped CuO-Based Catalysts Supported on Mesoporous $Ce_{0.8}Zr_{0.2}O_2$ with Intensified Low-Temperature Activity. *Catalysts* **2019**, *9*, 724. [CrossRef]
11. Bansmann, J.; Abdel-Mageed, A.M.; Chen, S.; Fauth, C.; Häring, T.; Kucerová, G.; Wang, Y.; Behm, R.J. Chemical and Electronic Changes of the CeO2 Support during CO Oxidation on $Au/CeO_2$ Catalysts: Time-Resolved Operando XAS at the Ce LIII Edge. *Catalysts* **2019**, *9*, 785. [CrossRef]
12. Sui, C.; Xing, L.; Cai, X.; Wang, Y.; Zhou, Q.; Li, M. Co-Supported $CeO_2$ Nanoparticles for CO Catalytic Oxidation: Effects of Different Synthesis Methods on Catalytic Performance. *Catalysts* **2020**, *10*, 243. [CrossRef]
13. Kaneti, Y.V.; Tanaka, S.; Jikihara, Y.; Nakayama, T.; Bando, Y.; Haruta, M. Room Temperature Carbon Monoxide Oxidation Based on Two-dimensional Gold-loaded Mesoporous Iron Oxide Nanoflakes. *Chem. Commun.* **2018**, *54*, 8514–8517. [CrossRef] [PubMed]
14. Zanella, R.; Giorgio, S.; Henry, C.R.; Louis, C. Alternative methods for the preparation of gold nanoparticles supported on $TiO_2$. *J. Phys. Chem. B* **2002**, *106*, 7634–7642. [CrossRef]
15. Bamwenda, G.R.; Tsubota, S.; Nakamura, T.; Haruta, M. The influence of the preparation methods on the catalytic activity of platinum and gold supported on $TiO_2$ for CO oxidation. *Catal. Lett.* **1997**, *44*, 83–87. [CrossRef]
16. Grunwaldt, J.D.; Kiener, C.; Wögerbauer, C.; Baiker, A. Preparation of supported gold catalysts for low-temperature CO oxidation via "size-controlled" gold colloids. *J. Catal.* **1999**, *181*, 223–232. [CrossRef]
17. Ivanova, S.; Petit, C.; Pitchon, V. A new preparation method for the formation of gold nanoparticles on an oxide support. *Appl. Catal. A Gen.* **2004**, *267*, 191–201. [CrossRef]
18. Dobrosz, I.; Jiratova, K.; Pitchon, V.; Rynkowski, J.M. Effect of the preparation of supported gold particles on the catalytic activity in CO oxidation reaction. *J. Mol. Catal. A Chem.* **2005**, *234*, 187–197. [CrossRef]
19. Rynkowski, J.M.; Dobrosz-Gómez, I. Ceria-Zirconia Supported Gold Catalysts. Annales Universitatis Mariae Curie-Skłodowska. *Ann. UMCS Chem.* **2009**, *64*, 197–217.
20. Trovarelli, A.; Fornasiero, P. (Eds.) *Catalysis by Ceria and Related Materials*, 2nd ed.; Imperial College Press: London, UK, 2013.

21. Dobrosz-Gómez, I.; Kocemba, I.; Rynkowski, J.M. Au/$Ce_{1-x}Zr_xO_2$ as effective catalysts for low-temperature CO oxidation. *Appl. Catal. B Environ.* **2008**, *83*, 240–255. [CrossRef]
22. Dobrosz-Gómez, I.; Gómez-García, M.Á.; Szynkowska, M.I.; Kocemba, I.; Rynkowski, J.M. Surface, structural and morphological characterization of nanocrystalline ceria–zirconia mixed oxides upon thermal aging. *Catal. Today* **2012**, *191*, 142–145. [CrossRef]
23. Dobrosz, I.; Gómez-García, M.Á.; Kocemba, I.; Maniukiewicz, W.; Rynkowski, J.M. Characterization of Au/$Ce_{1-x}Zr_xO_2$ catalysts in CO oxidation. *Polish J. Environ. Studies* **2005**, *14*, 231–234.
24. Dobrosz-Gómez, I.; Kocemba, I.; Rynkowski, J.M. Factors influencing structure and catalytic activity of Au/$Ce_{1-x}Zr_xO_2$ catalysts in CO oxidation. *Appl. Catal. B Environ.* **2009**, *88*, 83–97. [CrossRef]
25. Daturi, M.; Binet, C.; Lavalley, J.C.; Blanchard, G. Surface FTIR investigations on $Ce_xZr_{1-x}O_2$ system. *Surf. Interface. Anal.* **2000**, *30*, 273–277. [CrossRef]
26. Su, X.; Yang, X.F.; Huang, Y.Q.; Liu, B.; Zhang, T. Single-Atom Catalysis toward Efficient $CO_2$ Conversion to CO and Formate Products. *Acc. Chem. Res.* **2019**, *52*, 656–664. [CrossRef]
27. Wang, W.W.; Du, P.P.; Zou, S.H.; He, H.Y.; Wang, R.X.; Jin, Z.; Shi, S.; Huang, Y.Y.; Si, R.; Song, Q.S.; et al. Highly Dispersed Copper Oxide Clusters as Active Species in Copper-Ceria Catalyst for Preferential Oxidation of Carbon Monoxide. *ACS Catal.* **2015**, *5*, 2088–2099. [CrossRef]
28. Esrafili, M.D.; Mousavian, P. A DFT Study on the Possibility of Using A Single Cu Atom Incorporated Nitrogen-Doped Graphene as A Promising and Highly Active Catalyst for Oxidation of CO. *Int. J. Quant. Chem.* **2019**, *119*, e25857. [CrossRef]
29. Wang, H.; Shen, J.H.; Huang, J.F.; Xu, T.J.; Zhu, J.R.; Zhu, Y.H.; Li, C.Z. Atomically Dispersed Au Catalysts Supported on $CeO_2$ Foam: Controllable Synthesis and CO Oxidation Reaction Mechanism. *Nanoscale* **2017**, *9*, 16817–16825. [CrossRef]
30. Qiao, B.T.; Liu, J.X.; Wang, Y.G.; Lin, Q.Q.; Liu, X.Y.; Wang, A.Q.; Li, J.; Zhang, T.; Liu, J.Y. Highly Efficient Catalysis of Preferential Oxidation of CO in $H_2$-Rich Stream by Gold Single-Atom Catalysts. *ACS Catal.* **2015**, *5*, 6249–6254. [CrossRef]
31. Al Soubaihi, R.M.; Saoud, K.M.; Dutta, J. Critical Review of Low-Temperature CO Oxidation and Hysteresis Phenomenon on Heterogeneous Catalysts. *Catalysts* **2018**, *8*, 660. [CrossRef]
32. Tang, Y.; Wang, Y.-G.; Li, J. Theoretical Investigations of Pt-CeO2 Single-Atom Catalyst for CO Oxidation. *J. Phys. Chem. C.* **2017**, *121*, 11281–11289. [CrossRef]
33. Feng, Y.X.; Wang, Q.; Xiong, H.F.; Zhou, S.L.; Chen, X.; Hernandez, X.I.P.; Wang, Y.; Lin, S.; Datye, A.K.; Guo, H. Correlating DFT Calculations with CO Oxidation Reactivity on Ga-Doped Pt/$CeO_2$ Single-Atom Catalysts. *J. Phys. Chem. C* **2018**, *122*, 22460–22468. [CrossRef]
34. Kropp, T.; Lu, Z.; Li, Z.; Chin, Y.-H.C.; Mavrikakis, M. Anionic Single-Atom Catalysts for CO Oxidation: Support-Independent Activity at Low Temperatures. *ACS Catal.* **2019**, *9*, 1595–1604. [CrossRef]
35. Yu, M.; Feng, Y.; Gao, L.; Lin, S. Phosphomolybdic Acid Supported Single-Metal-Atom Catalysis in CO Oxidation: First-Principles Calculations. *Phys. Chem. Chem. Phys.* **2018**, *20*, 20661–20668. [CrossRef]
36. Wang, S.; Feng, Y.; Lin, S.; Guo, H. Phosphomolybdic Acid Supported Atomically Dispersed Transition Metal Atoms (M = Fe, Co, Ni, Cu, Ru, Rh, Pd, Ag, Os, Ir, Pt, and Au): Stable Single Atom Catalysts Studied by Density Functional Theory. *RSC Adv.* **2017**, *7*, 24925–24932. [CrossRef]
37. Liu, X.; Sui, Y.H.; Duan, T.; Meng, C.G.; Han, Y. CO Oxidation Catalyzed by Pt-Embedded Graphene: A First-Principles Investigation. *Phys. Chem. Chem. Phys.* **2014**, *16*, 23584–23593. [CrossRef]
38. Tang, Y.N.; Dai, X.Q.; Yang, Z.X.; Pan, L.J.; Chen, W.G.; Ma, D.W.; Lu, Z.S. Formation and Catalytic Activity of Pt Supported on Oxidized Graphene for the CO Oxidation Reaction. *Phys. Chem. Chem. Phys.* **2014**, *16*, 7887–7895. [CrossRef]
39. Morgan, K.; Cole, K.J.; Goguet, A.; Hardacre, C.; Hutchings, G.J.; Maguire, N.; Shekhtman, S.O.; Taylor, S.H. TAP studies of CO oxidation over $CuMnO_X$ and Au/$CuMnO_X$ catalysts. *J. Catal.* **2010**, *276*, 38–48. [CrossRef]
40. Schlexer, P.; Widmann, D.; Behm, R.J.; Pacchioni, G. CO Oxidation on a Au/$TiO_2$ Nanoparticle Catalyst via the Au-Assisted Mars–van Krevelen Mechanism. *ACS Catal.* **2018**, *8*, 6513–6525. [CrossRef]
41. Saqlain, M.A.; Hussain, A.; Siddiq, M.; Leitao, A.A. A DFT+U study of the Mars van Krevelen Mechanism of CO Oxidation on Au/$TiO_2$ catalysts. *Appl. Catal. A* **2016**, *519*, 27–33. [CrossRef]
42. Duan, Z.; Henkelman, G. CO Oxidation at the Au/$TiO_2$ Boundary: The Role of the Au/$Ti_{5c}$ Site. *ACS Catal.* **2015**, *5*, 1589. [CrossRef]

43. Widmann, D.; Behm, R.J. Activation of Molecular Oxygen and the Nature of the Active Oxygen Species for CO Oxidation on Oxide Supported Au Catalysts. *Acc. Chem. Res.* **2014**, *47*, 740–749. [CrossRef]
44. Dobrosz, I.; Kocemba, I.; Rynkowski, J.M. The Optimisation of Au/$Ce_{0.75}Zr_{0.25}O_2$ Catalyst Preparation for CO Oxidation. *Pol. J. Environ. Studies* **2006**, *15*, 44.
45. Dobrosz-Gómez, I.; Kocemba, I.; Rynkowski, J.M. Carbon Monoxide Oxidation over Au/$Ce_{1-x}Zr_xO_2$ Catalysts: Effects of Moisture Content in the Reactant Gas and Catalyst Pretreatment. *Catal. Lett.* **2009**, *128*, 297–306. [CrossRef]
46. Dobrosz-Gómez, I.; Gómez-García, M.Á.; Rynkowski, J.M. The Role of Au-Support Interactions in Creation of Catalytic Performance of Au/$Ce_{0.75}Zr_{0.25}O_2$ in CO Oxidation. *Pol. J. Environ. Studies* **2009**, *18*, 587–591.
47. Dobrosz-Gómez, I.; Gómez-García, M.Á.; Rynkowski, J.M. CO Oxidation over Au/$CeO_2$–$ZrO_2$ Catalysts: The Effect of the Support Composition of the Au Support Interaction. *Kinet. Catal.* **2010**, *51*, 823–827. [CrossRef]
48. Gómez-García, M.Á.; Gómez-Mendoza, N.A.; Dobrosz-Gómez, I.; Gil Pavas, E.; Rynkowski, J.M. Temperature-Scanning Method for the Kinetic Studies of CO Oxidation over Ceria–Zirconia Supported Gold Catalysts. *Chem. Eng. J.* **2015**, *282*, 20–28. [CrossRef]
49. Force, C.; Belzunegui, J.P.; Sanz, J.; Martinez-Arias, A.; Soria, J. Influence of precursor salt on metal particle formation in Rh/$CeO_2$ catalysts. *J. Catal.* **2001**, *197*, 192–199. [CrossRef]
50. Ivanova, S.; Pitchon, V.; Zimmermann, Y.; Petit, C. Preparation of alumina supported gold catalysts: Influence of washing procedures, mechanism of particles size growth. *Appl. Catal. A Gen.* **2006**, *298*, 57–64. [CrossRef]
51. Schulz, A.; Hargittai, M. Structural variations and bonding in gold halides: A quantum chemical study of monometric and dimetric gold monohalide and gold trihalide molecules, AuX, $Au_2X_2$, $AuX_3$, and $Au_2X_6$ (X = F, Cl, Br, I). *Chem. Eur. J.* **2001**, *7*, 3657–3670. [CrossRef]
52. Arena, F.; Famulari, P.; Trunfio, G.; Bonura, G.; Frusteri, F.; Spadaro, L. Physicochemical properties and reactivity of Au/CeO2 catalysts in total and selective oxidation of CO. *Appl. Catal. B Environ.* **2006**, *66*, 81–91. [CrossRef]
53. Fu, L.; Wu, N.Q.; Yang, J.H.; Qu, F.; Johnson, D.L.; Kung, M.C.; Kung, H.H.; Dravid, V.P. Direct evidence of oxidized gold on supported gold catalysts. *J. Phys. Chem. Lett. B* **2005**, *109*, 3704–3706. [CrossRef]
54. Cao, A.; Lu, R.; Veser, G. Stabilizing Metal Nanoparticles for Heterogeneous Catalysis. *Phys. Chem. Chem. Phys.* **2010**, *12*, 13499–13510. [CrossRef]
55. Cuenya, B.R. Synthesis and Catalytic Properties of Metal Nanoparticles: Size, Shape, Support, Composition, and Oxidation State Effects. *Thin Solid Films* **2010**, *518*, 3127–3150. [CrossRef]
56. Jóźwiak, W.K.; Kaczmarek, E.; Ignaczak, W. Activity requirements of gold catalysts Au/$Fe_2O_3$ in low-temperature CO oxidation. *Pol. J. Environ. Studies* **2005**, *14*, 127.
57. Moreau, F.; Bond, G.C.; Taylor, A.O. Gold on Titania Catalysts for the Oxidation of Carbon Monoxide: Control of PH during Preparation with Various Gold Contents. *J. Catal.* **2005**, *231*, 105–114. [CrossRef]
58. Zanella, R.; Delannoy, L.; Louis, C. Mechanism of Deposition of Gold Precursors onto $TiO_2$ during the Preparation by Cation Adsorption and Deposition–Precipitation with NaOH and Urea. *Appl. Catal. A* **2005**, *291*, 62–72. [CrossRef]
59. Grzybowska-Świerkosz, B. Nano-Au/oxide Support Catalysts in Oxidation Reactions: Provenance of Active Oxygen Species. *Catal. Today* **2006**, *112*, 3–7. [CrossRef]
60. Guzmán, J.; Carrettin, S.; Corma, A. Spectroscopic evidence for the supply of reactive oxygen during CO oxidation catalyzed by gold supported on nanocrystalline $CeO_2$. *J. Am. Chem. Soc.* **2005**, *127*, 3286–3287. [CrossRef]
61. Cunningham, D.A.H.; Vogel, W.; Haruta, M. Structural analysis of Au/$TiO_2$ catalysts by debye function analysis. *Catal. Lett.* **1999**, *63*, 43–47. [CrossRef]
62. Olea, M.; Tada, M.; Iwasawa, Y. TAP study on carbon monoxide oxidation over supported gold catalysts Au/Ti(OH)*$_4$ and Au/Fe(OH)*$_3$: Moisture effect. *J. Catal.* **2007**, *248*, 60–67. [CrossRef]
63. Costello, C.K.; Yang, J.H.; Law, H.Y.; Wang, Y.; Lin, J.-N.; Marks, L.D.; Kung, M.C.; Kung, H.H. On the potential role of hydroxyl groups in CO oxidation over Au/$Al_2O_3$. *Appl. Catal. A. Gen.* **2003**, *243*, 15–24. [CrossRef]
64. Ruszel, M.; Grzybowska, B.; Samson, K.; Gressel, I.; Klisinska, A. MII$Cr_2O_4$-spinels as supports for Au nanoparticles in oxidation of CO. *Catal. Today* **2006**, *112*, 126–129. [CrossRef]
65. Kang, Y.-M.; Wan, B.-Z. Gold and iron supported on Y-type zeolite for carbon monoxide oxidation. *Catal. Today* **1997**, *35*, 379–392. [CrossRef]

66. Visco, A.M.; Neri, F.; Neri, G.; Donato, A.; Milone, C.; Galvagno, S.X. X-ray photoelectron spectroscopy of $Au/Fe_2O_3$ catalysts. *Phys. Chem. Chem. Phys.* **1999**, *1*, 2869–2873. [CrossRef]
67. Pillai, U.R.; Deevi, S. Highly active gold-ceria catalyst for the room temperature oxidation of carbon monoxide. *Appl. Catal. A Gen.* **2006**, *299*, 266–273. [CrossRef]
68. Abd El-Moemen, A.; Karpenko, A.; Denkwitz, Y.; Behm, R.J. Activity, stability and deactivation behavior of $Au/CeO_2$ catalysts in the water gas shift reaction at increased reaction temperature (300 °C). *J. Power Sources* **2009**, *190*, 64–75. [CrossRef]
69. Widmann, D.; Leppelt, R.; Behm, R.J. Activation of a $Au/CeO_2$ catalyst for the CO oxidation reaction by surface oxygen removal/oxygen vacancy formation. *J. Catal.* **2007**, *251*, 437–442. [CrossRef]
70. Wang, A.Q.; Hsieh, Y.P.; Chen, Y.F.; Mou, C.Y. Au–Ag alloy nanoparticle as catalyst for CO oxidation: Effect of Si/Al ratio of mesoporous support. *J. Catal.* **2006**, *237*, 197–206. [CrossRef]
71. Qian, K.; Huang, W.; Fang, J.; Lv, S.; He, B.; Jiang, Z.; Wei, S. Low-temperature CO oxidation over $Au/ZnO/SiO_2$ catalysts: Some mechanism insights. *J. Catal.* **2008**, *255*, 269–278. [CrossRef]
72. del Río, E.; Collins, S.E.; Aguirre, A.; Chen, X.; Delgado, J.J.; Calvino, J.J.; Bernal, S. Reversible deactivation of a $Au/Ce_0.62Zr0.38O2$ catalyst in CO oxidation: A systematic study of $CO_2$-triggered carbonate inhibition. *J. Catal.* **2014**, *316*, 210–218. [CrossRef]
73. Provendier, H.; Petit, C.; Schmitt, J.L.; Kiennemann, A.; Chaumont, C. Characterization of the solid solution $La(Ni,Fe)O_3$ prepared via sol-gel related method using propionic acid. *J. Mat. Sci.* **1999**, *34*, 4121–4127. [CrossRef]
74. Johnson, M.F.L.; Mooi, J. Cerium dioxide crystallite sizes by temperature-programmed reduction. *J. Catal.* **1987**, *103*, 502. [CrossRef]
75. Johnson, M.F.L.; Mooi, J. Cerium dioxide crystallite sizes by temperature-programmed reduction. *J. Catal.* **1993**, *140*, 612. [CrossRef]